2. EXPERIMENTS

2.1 Nuclear Reactions

2.1.1 Excitation of the 2^+ (E^*=2.7 MeV) state in ^{56}Ni by inelastic proton scattering

J. Friese, A. Gillitzer, H.-J. Körner, M. Peter, L.V. Chulkov [d], P. Egelhof [a], C. Fischer [a], H. Geissel [a], M. Golovkov [b], W. Henning [b], A. Himmler [a], J.V. Kratz [c], G. Kraus [a], F. Nickel [a], G. Münzenberg [a], A.A. Ogloblin [b], J.P. Schiffer [b], W. Schwab [a], A. Weiß [a]
[a] GSI, Darmstadt
[b] ANL, Argonne, Illinois
[c] U. Mainz
[d] I.V. Kurchatov Inst., Moskau

Radioactive beams from the heavy-ion synchrotron SIS (GSI, Darmstadt) in combination with the projectile fragment separator FRS [1] open the possibility for nuclear structure studies with direct reactions on unstable nuclei. Planned experiments include measurements of elastic and inelastic proton-scattering and transfer reactions such as (d, p), (d, t), etc. on nuclei in the vicinity of the doubly magic isotopes ^{56}Ni and ^{132}Sn and in a region of astrophysical interest around A=50 [2]. In a first experiment we investigated (p, p$'$) - inelastic scattering on ^{56}Ni to the first excited 2^+ ($E^* = 2.7\,MeV$) state at an incident energy of E_{lab} = 101 MeV/u. The measurement was intended to yield a more accurate value of the poorly known [3] matrix element for the transition from the 0^+-ground state. Furtheron, the measurement provided an experimental test of the problems associated with the study of reactions using radioactive beams in inverse kinematics.

The first diffraction maximum of the angular distribution of the differential cross-section for the excitation to the 2^+ ($E^* = 2.7\,MeV$) state in ^{56}Ni (expected at $\Theta_{CM} = 12°$ - $18°$ [5]) is localized between $\theta_{lab} = 78.5°$ and $\theta_{lab} = 80.9°$ in the laboratory system (inverse kinematics !). Due to the large level spacing in ^{56}Ni and the moderate kinematical variation of the recoil energy with laboratory angle, the inelastically scattered protons of interest are energetically well separated from the elastic protons. Hence, a large angular acceptance of the detector system ($\Delta\,\theta_{lab} = 2°$), as well as a comparatively large energy spread of the incident beam could be tolerated. As no additional cooling of the secondary beam in the ESR was needed, we performed the experiment at the final focal plane (S4) of the FRS. The ^{56}Ni -beam was produced by fragmentation of $350\,A \cdot MeV$ ^{58}Ni projectiles on a $4\,g/cm^2$ beryllium target. The fragment separator was tuned in an achromatic mode using a thin aluminum wedge degrader at the central focal plane (S2).

The experimental setup (except for the FRS part) is shown in Fig. 1. Total energy and time of flight of the recoiling protons were measured with 18 silicon detectors (48 × 8 mm^2 active area each, 2500 μm thick). The detectors were assembled in a vacuum chamber on a concentric ring of 20 cm radius around a 1 mg/cm^2 $(CH_2)_n$ -target. The target was mounted on a linear translation stage and could be moved along the beam axis. Thus a range of laboratory angles $77.5° \leq \theta_{lab} \leq 83.0°$ could be covered. A set of scintillation detectors was used to track the beam particles and to identify their nuclear charge and mass by time of flight and energy loss measurements. In order to minimize secondary reactions and multiple scattering all scintillators were mounted in vacuum chambers. The TOF start

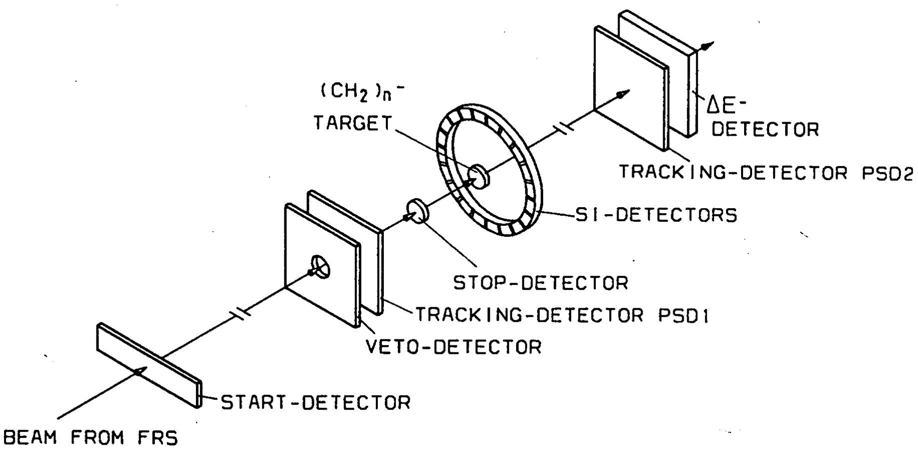

Fig. 1: Schematical view of the experimental setup at the FRS (for details see text).

signal was obtained from a position sensitive scintillator placed behind the degrader at S2. The tracking detectors, two $2-dim$ position sensitive scintillators (PSD1 and PSD2, 140 × 140 mm^2 active area, read out with four photomultipliers) were mounted up- and downstream from the target. The whole scintillation detector system allowed for maximum beam intensities up to $10^5\,sec^{-1}$. A position resolution of $\Delta x = \Delta y \approx 1\,mm$ and a time resolution of $\Delta t \approx 250\,ps$ was achieved. A well separated ^{56}Ni -beam with an intensity of up to $3\times10^4\,sec^{-1}$ and an emittancy of $\epsilon \approx 26\,\pi$ mmmrad on target was obtained.

The low energetic recoiling protons were identified by an energy and time of flight measurement (time resolution ≈ 3 ns). The background originating from ^{56}Ni + ^{12}C collisions was measured with a ^{12}C-target and subtracted from the yield obtained with the 1 mg/cm^2 $(CH_2)_n$ -target. The scattering angle for each proton was deduced from the projectile tracking-data with sufficient accuracy. Thus a separation of elastic and inelastic protons was achieved. Corrections for energy-loss and multiple scattering in the 1 mg/cm^2 $(CH_2)_n$ are included. As a result of this data analysis in Fig. 2 (upper part, right-hand side) the energy spectrum of the scattered protons is displayed.

The spectrum reveals two main contributions in regions, where the elastic and inelastic yields are expected. Due to the good detector energy resolution, the intensity distribution within each of the two regions reflects directly the angular distribution of the scattered protons in the angular acceptance of the detector aperture. The shape of the spectrum is fairly reproduced by a Monte-Carlo simulation (lower part, right-hand side of Fig. 2) taking into account a proper reaction mechanism and all experimental constraints. The yield of the emerging protons was extracted from optical model [4] and CCBA calculations assuming a value $\beta_2 = 0.2$ for the 2^+ $(E^* = 2.7\,MeV)$ state. The angular cut for inelastic scattering covers the first diffraction maximum, for elastic scattering it is near a calculated minimum in the angular distribution.

The experimental procedure and the validity of the data-analysis was tested by elastic proton-scattering with a stable ^{58}Ni beam. The results are shown in the left part of Fig. 2. The comparison of the measured spectra to calculations based on data from the literature [4] yields an excellent agreement for the deduced cross-sections.

From the analysis of the ^{56}Ni -data we extract a value of $(\frac{d\sigma}{d\Omega}) = 18.5$ mb/sr with a 4.5 % statistical error for the inelastic cross-section in the diffraction maximum and $(\frac{d\sigma}{d\Omega}) = 26.2$ mb/sr with a 3.6 % statistical error for the elastic cross-section in the diffraction minimum. The corresponding

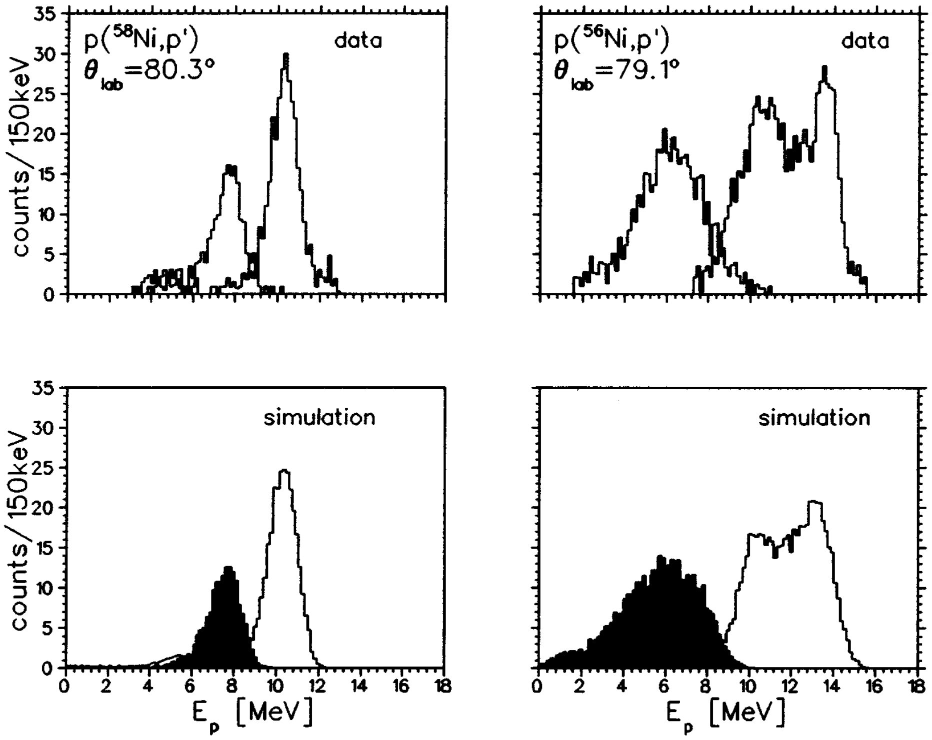

Fig. 2: Measured energy spectra (upper part) for p (^{58}Ni, p')^{58}Ni* at 114 MeV/u, θ_{lab} = 80.3 ± 0.3 ° (left) and p (^{56}Ni, p')^{56}Ni* at 101 MeV/u, θ_{lab} = 79.1 ± 0.9 ° (right) in comparison with the expected spectra obtained from Monte-Carlo simulations (lower part). The spectra are normalized in vertical scale.

β_2= 0.21(2) – including systematical errors – allows to deduce the matrix element for the transition connecting the 0^+-ground state to the 2^+-first excited state of ^{56}Ni with an accuracy of about 10 %. Assuming a uniform charge-distribution, the extracted value is $B(E2)$ = 850(120) e^{2}fm^4. This value has to be compared to the limit $B(E2) \geq 230$ e^{2}fm^4 from ref.[3].

In this experiment we have shown that the study of direct reaction mechanisms with radioactive heavy projectiles is a feasible tool to investigate the nuclear structure of unstable isotopes. With increasing primary beam intensities and additional beam cooling in the experimental storage ring ESR even nuclei further off the valley of stability are accessible.

[1] B. Franzke et al., *Proc. 3rd European Particle Accelerator Conference*, Berlin, 1992, to be published
[2] P. Egelhof, *Proc. Int. Workshop on the Physics and Techniques of Secondary Nuclear Beams*, Dourdan, France, 1992, (J.F. Bruandet, B. Fernandez, M. Bex, eds.), Editions Frontieres, 1992, p.217
[3] S. Raman et al., *Atomic Data Nuclear Data Tables* 36(1987)1
[4] K. Kwiatkowski et al., *Nuclear Physics A* 301(1978)349
[5] L.W. Woo et al., *Physical Review C* 29(1984)794

2.1.2 Fragmentation products of secondary ^{56}Ni projectiles measured with a SISWICH

J. Friese, A. Gillitzer, H.-J. Körner, M. Peter, J. Reinhold

Phoswich counters [1] – i.e. two scintillators with different light output decay times sandwiched together and viewed by one photo multiplier tube – have found widespread use as detectors for medium energy particles [2, 3, 4, 5]. They provide moderate energy resolution and particle identification up to atomic numbers $Z = 20$. But they somewhat suffer from two inherent characteristics of the scintillator materials used. First, the light output per unit of energy deposit of the thin ΔE plastic scintillator is small compared to that of the residual energy measuring crystal (i.e. CsI(Tl)) [6].

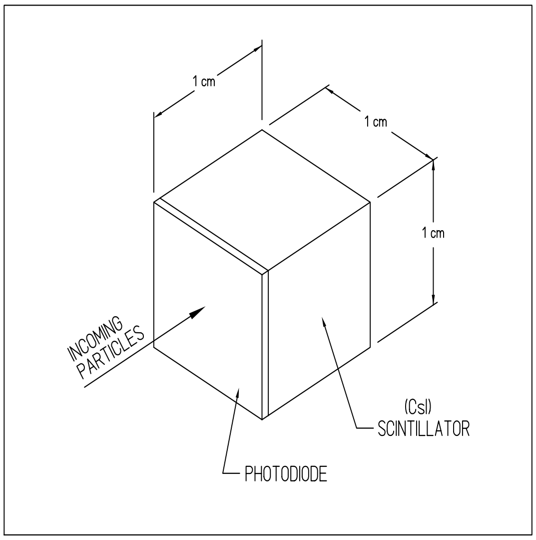

Fig. 1: Schematic view of the SISWICH detector

Second, the response of scintillators to different particles is nonlinear, and depends significantly on the atomic number Z and the operating temperature of the device [7]. An additional complication is the gain instability and limited dynamic range of photo multiplier tubes, which at least requires light pulser calibration techniques [2, 7]. However, the energy loss to light conversion is not tested by these methods.
To overcome the calibration, stability, and dynamic range problems, we have replaced the front plastic scintillator by a silicon PIN photo diode [9]. Fig. 1 illustrates schematically a so called SISWICH (Silicon Scintillator Sandwich) detector.

The photo diode measures both, the energy loss of the traversing particle and the light output of the glued on CsI(Tl) - crystal. The signal delivered contains basically two contributions, a fast component ($\tau \simeq 10\,$ns) corresponding to the electronic charge produced directly in the depletion layer of the silicon diode, and a slow ($\tau \simeq 1.0\,\mu$s) component resulting from the scintillation light decay in the CsI(Tl). Providing two different shaping time constants in the output signal processing thus yields the ΔE and the $\Delta\mathrm{E} + \mathrm{E}_{res}$ information. The most promising advantage of this device is the calibration capability of the silicon detector [8] which in turn also allows an unambiguous energy determination from the scintillator signal. Additionaly, SISWICH detectors can be operated in any magnetic field environment, in contrast to PHOSWICHes.

For light ions we have shown the feasibility of such a one element detector telescope [10]. In order to test its response to high energy heavy ions we have performed measurements at the GSI, Darmstadt.

At the fragment separator FRS a secondary ^{56}Ni beam was produced by the fragmentation of 350 A·MeV ^{58}Ni projectiles. The experimental setup and other details are presented in this report [11]. At the end of the evacuated FRS beamline we have placed - under very forward angles with repect to the beam direction - a SISWICH, consisting of a $220\,\mu$m thick photo diode (Siemens, F109D) and a $1 \cdot 1 \cdot 1\,cm^3$ CsI(Tl) - crystal (Bicron). The beamline exit window, a $200\,\mu$m titanium foil, and a

Fig. 2: Measured pulse heights τ_{short} vs. τ_{long} for reaction products of 4.5 GeV ^{56}Ni on ^{nat}Ti.

2 mm thick Ne102 scintillator served as a secondary target. The ^{56}Ni projectiles were decelerated by the production target, the degrader, and upstream detectors down to energies $E_{Proj} \simeq 80\,A{\cdot}MeV$. The reaction products were decelerated further to $E_{Frag} \simeq 30 - 50\,A{\cdot}MeV$ by the titanium foil, the air along the flight path, the Ne102, and the light protection entrance window in front of the detector.

The detector signal was read out with a commercial preamplifier (Canb. 2003BT) and two spectroscopy amplifiers (Canb. 2021) with peaking times $\tau_{short} = 0.5\,\mu sec$ and $\tau_{long} = 8\,\mu sec$. Fig. 2 shows a two dimensional display of the fast versus the slow signal.

Fig. 3: ΔE - E_{tot} spectrum in arbitr. units calculated from Fig. 2. The particular structure in the projectile region is due to contaminations in the secondary ^{56}Ni - beam and to scattering in upstream transmission detectors.

In a first order approximation the particle energy loss and residual energy can easily be deduced from the two pulse heights [9, 10]. The result is illustrated in Fig. 3 as a ΔE versus E_{tot} spectrum. The identification power for elements up to $Z = 28$, as shown in Fig. 4, is impressive, in spite of the non optimum measurement conditions. A mere energy loss measurement could not have yielded element identification at these particle energies.

We have shown that the SISWICH is a versatile, compact, and rugged particle detector for identifying light to heavy ions with energies ≥ 5 MeV/nucleon. It should be stressed, that due to the high resolving power of silicon PIN photo diodes even for heavier ions [10], the SISWICH is a very useful, easy to handle and low cost device for measurements of medium energy heavy ions up to $Z \leq 60$.

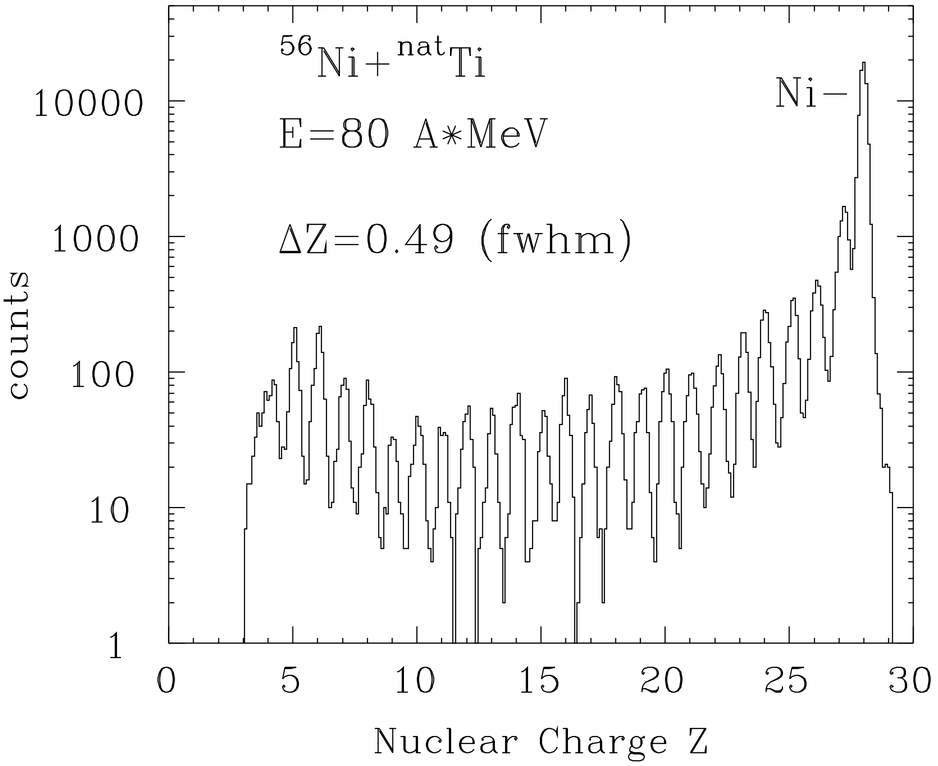

Fig. 4: Extracted atomic number spectrum for the heavy reaction products of 4.5 GeV ^{56}Ni - projectiles on titanium and Ne102. Ions with $Z \leq 4$ are not stopped in the detector.

[1] D.H. Wilkinson, Rev. Sci. Instr. 23 (1952) 415
[2] A. Baden et al., Nucl. Instr. Meth. 203 (1982) 189
[3] A. Bantel et al., Nucl. Instr. Meth. 226 (1984) 394
[4] G.D. Westfall, Nucl. Instr. Meth. A238 (1985) 347
[5] D.G. Sarantites et al., Nucl. Instr. Meth. A264 (1988) 319
[6] J. Alarja et al., Nucl. Instr. Meth. A242 (1986) 352
[7] P. Stracener et al., Nucl. Instr. Meth. A294 (1990) 485
[8] H. Spieler, IEEE Trans. Nuc. Sci. NS29 (1982) 1142
[9] J. Friese et.al., IEEE Nucl. Sci. Symp., Orlando 1992, Proceedings
[10] J. Friese et.al., Annual Report (1990) 192, 195
[11] J. Friese et.al., contribution to this report

2.1.3 Production of Proton Rich Nuclei by Fragmentation of ^{58}Ni at 350 A·MeV

J. Friese, A. Gillitzer, H.-J. Körner, M. Peter, L.V. Chulkov [d], P. Egelhof [a], C. Fischer [a], H. Geissel [a], M. Golovkov [b], W. Henning [b], J.V. Kratz [c], G. Kraus [a], A. Magel [a], F. Nickel [a], G. Münzenberg [a], A.A. Ogloblin [b], J.P. Schiffer [b], W. Schwab [a], A. Weiß [a]
[a] GSI, Darmstadt
[b] ANL, Argonne, Illinois
[c] U. Mainz
[d] I.V. Kurchatov Inst., Moskau

At the fragment separator FRS secondary beams in the mass region $42 < A < 57$ were produced by the fragmentation of 350 A·MeV ^{58}Ni projectiles. The primary beam was delivered by the UNILAC-SIS accelerator complex at GSI, Darmstadt. The aim of this experiment was twofolded. At first the production of an isotopically clean ^{56}Ni beam with low emittancy was essential for nuclear structure studies using (p,p′) inelastic proton scattering in inverse kinematic [1]. The thickness of the production target, the FRS setup and the proper choice of the degrader were optimized with the help of MOCADI calculations [2, 3] to give a maximum number of well separated ^{56}Ni fragments per spill. We used a 4 g/cm^2 beryllium production target and a thin ($4.2\,mm$ Al) achromatic degrader at the dispersive central focal plane (S2) to achieve these conditions. The second part of the experiment was dedicated to the measurement of production cross sections of very proton rich nuclei in the $A \simeq 50$ mass region. Furthermore we wanted to demonstrate the capability of fragment identification in the nickel mass region at high secondary beam intensities ($\approx 10^5$ particles/s). The online identification at moderate and high intensities is crucial for a considerable number of experiments using secondary beams at the final FRS focus. Products from secondary reactions in the degrader and upstream detectors might contaminate the beam species of interest to a non neglegible amount. This holds in particular for the low energy regime ($E_{Pro} \leq 200$ A·MeV), where the separation power of the FRS is reduced.

The experimental setup used is schematically shown in ref. [1]. The fragments were identified with a ΔE-TOF-B·ρ measurement. We used position sensitive plastic scintillators placed in vacuum housings at S2 and the final focal plane (S4). The flight path amounted to $L_{TOF} \simeq 36$ m. The scintillator at S2 (d = 1 mm) as well as the large ($A = 14 \cdot 14\,cm^2$) two dimensional position sensitive detector at S4 (d = 0.5 mm) achieved a position resolution of $\Delta x \approx \Delta y \approx 2$ mm (fwhm). A third position sensitive plastic scintillator placed 3 m downstream from the second detector at S4 allowed for tracking of the transmited fragments. The ΔE information was deduced from the pulse heights of both scintillators at S2 and S4. The overall resolution of the ΔE-TOF system was ΔTOF = 230 ps (fwhm), ΔZ = 0.85 (fwhm). Up to a maximum rate of $\approx 10^5$ particles/s of a quasi continuous beam no severe deterioration of the detector resolution was observed. At higher rates, tested with a primary ^{58}Ni beam, the obtained position as well as timing resolutions then rapidly decreased. Already an increase by a factor of 2 in the incident rate lead to values $\Delta x \approx \Delta y \geq 1\,cm$. Due to quenching of the PM-tubes at these rates the pulse height distributions heavily broadened. An energy loss of typically 300 MeV/fragment was deposited in each scintillator at S4, as the fragments were decelerated by the production target, the degrader, and upstream detectors down to energies $E_{Frag} \simeq 100$ A·MeV.

The magnetic rigidity B·ρ of the fragments was calculated from their positions at the central and final image plane with the information of the magnetic field strenghts measured by Hall probes. The resulting fragment mass numbers were determined with an accuracy ΔA = 1.2 (fwhm). A sample

ΔE-TOF spectrum is shown in Fig. 1 for a B$\cdot\rho$ setting with ^{52}Co spatially centered at the final focus. The separation of individual isotopes is clearly demonstrated. The production cross sections of proton rich-fragments in this mass region were successively determined with 6 different magnetic field settings of the FRS. Even for the weakest channels investigated ($\sigma \approx 10\,nb$) the data acquisition time did not exceed 1 hour at maximum primary beam intensities. A secondary electron transmission detector (SEETRAM) [4] located in front of the target served to measure the beam intensity for normalisation of the production yields. The measured count rates of the identified fragments were corrected by the deadtime of the data acquisition system and the efficiency of the detectors. Transmission losses in the FRS were evaluted from MOCADI calculations.

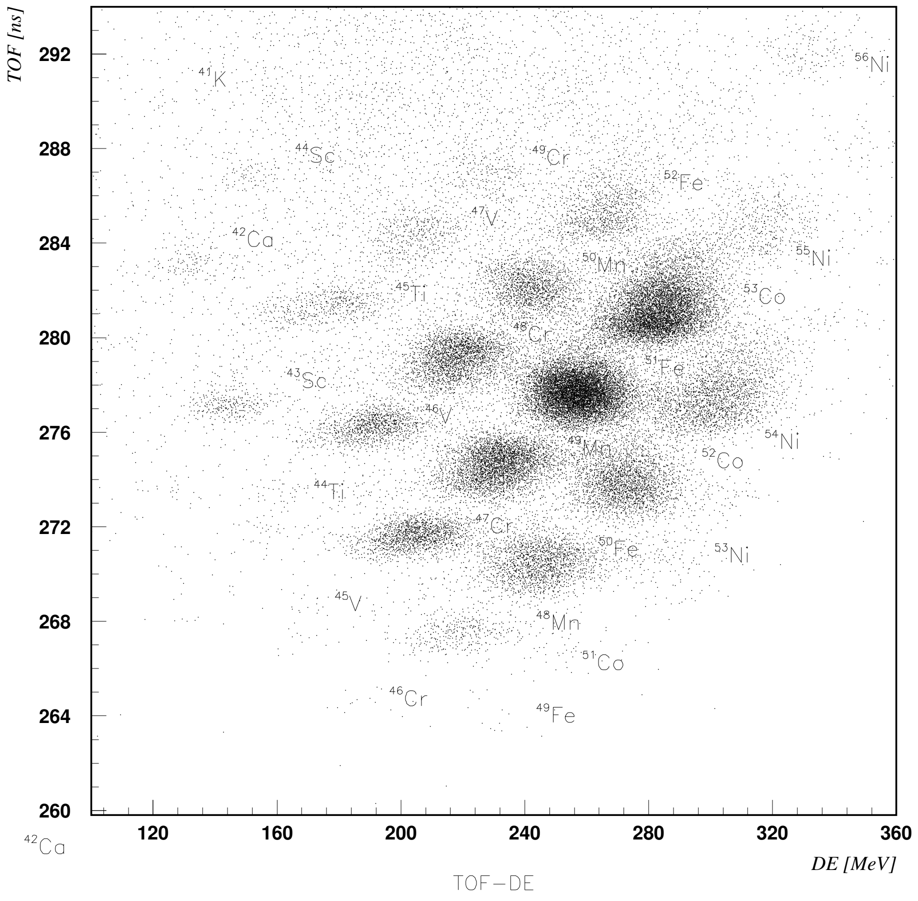

Fig. 1: TOF-ΔE spectrum for the magnetic setting on ^{52}Co. The identified fragments are marked.

Fig. 2 shows the experimental cross sections for nickel and cobalt isotopes in comparison to two model calculations. The full line denotes the empirical parametrization EPAX V1.1 [5], based on target fragmentation studies. The dashed line corresponds to the modified macroscopic abration-ablation model [6]. Calculations with the intra-nuclear-cascade (INC) code ISABEL [7] for the fast step and the PACE [8] code for the evaporation part are indicated by a dotted line. The calculations show a good overall agreement with the measured data except for the very proton rich isotopes, where they overestimate the data by nearly half an order of magnitude. A simular behaviour has also been observed in fragmentation of ^{129}Xe projectiles [9].

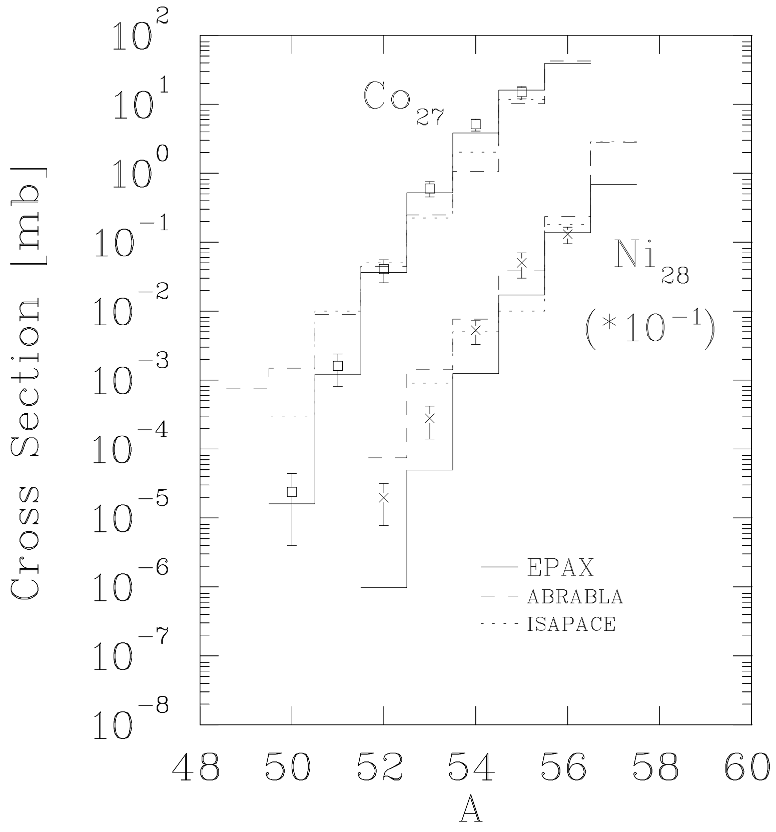

Fig. 2: Cross sections of Z=28 and Z=27 isotopes produced from 350 MeV/u ^{58}Ni on a 4 g/cm^2 ^{9}Be target in comparision to model calculations. Data points: measured values (this work), full lines: EPAX, dashed lines: statistical abrasion model, dotted lines: intranuclear-cascade model

[1] J. Friese et.al., contribution to this report
[2] Th. Schwab, Scientific Report GSI-91-10
[3] A. Magel, private communication
[4] C. Ziegler et.al. Scientific Report GSI-90-1 (1990) 257
[5] K. Sümmer et.al. Phys. Rev. **C42** (1990) 2546
[6] J.-J. Gaimard, K.H. Schmidt, Nucl. Phys. **A531** (1991) 709
[7] Y. Yariv, Z. Fraenkel, Phys. Rev. **C20** (1979) 2227
[8] M. Fauerbach, Diplomarbeit 1992, TH Darmstadt
[9] J. Friese et.al., contribution to this report

2.1.4 Excitations of ^{96}Zr from inelastic scattering experiments

D. Hofer, R. Hertenberger, E. Müller-Zanotti, W. Oelmaier, B. Valnion and G. Graw

The investigation of inelastic excitations of ^{96}Zr using 22 MeV protons and polarized deuterons with special view to two-octupole-phonon states has been completed now [1].

Further aspects of the excitation mechanism of two-octupole-phonon states are still of experimental and theoretical interest. Therefore an (α, α') experiment using 40 MeV α's and the Q3D magnetic spectrograph has been performed with an energy resolution of 12 keV FWHM. Fig. 1 shows a spectrum of the (α, α') reaction. The high resolution inelastic α scattering data are expected to give additional informations on sequential and direct excitation contributions of the two-octupole-phonon states in comparison with proton and deuteron scattering data.

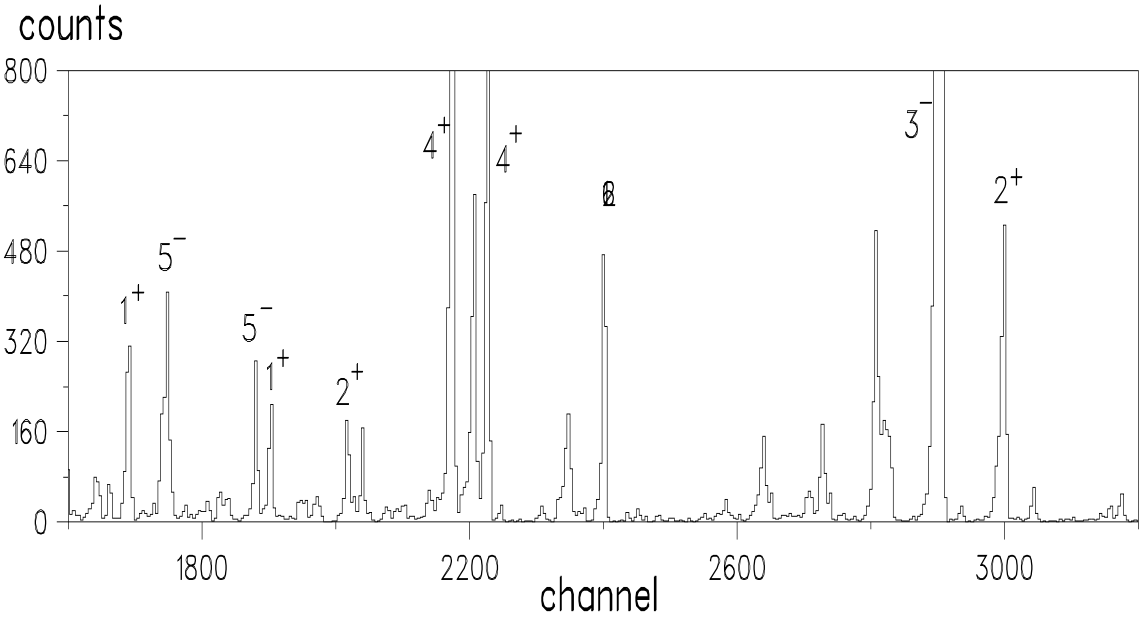

Fig. 1: ^{96}Zr (α, α'), $\theta_{lab} = 15^0$, $E_\alpha = 40$ MeV.

Calculations in a self-consistent quasiparticle-phonon-model to describe one-phonon, two-phonon and mixing of one- and two-phonon excitations in ^{96}Zr are in progress [2].

[1] D. Hofer et al., Nucl. Phys. A551 (1993) 173
[2] A. Platonov et al., Kurchatov Intitute Moscow, private communication (1992)

2.1.5 Excitations in ^{113}Cd from the (d,p) reaction.

Zs. Németh [a], D. Hofer, R. Hertenberger, E. Müller-Zanotti, B. Valnion, G. Graw
[a] Institute of Isotopes, Budapest, Hungary

^{113}Cd is a branching point in the astrophysical s-process. Both its $1/2^+$ ground state and its $11/2^-$ isomer at 263 keV excitation energy, which has a half-life of 14 y, are populated following neutron capture on ^{112}Cd. The predominant β-decay mode of the isomer results in a side path toward ^{113}In, which competes the main $^{112}Cd \rightarrow {}^{113g}Cd \rightarrow {}^{114}Cd$ branch. The effective branching ratio is sensitive to nuclear structure parameters of higher excited states, especially to the location of the low-lying gateway levels, since thermalization may occur in the hot stellar plasma [1]. For reliable s-process calculations detailed knowledge of the level scheme of ^{113}Cd is thus required.

^{113}Cd has recently been studied by Coulomb excitation [2], by the (n,n'γ) [3] and the (γ,γ') [4] reactions. An (α,nγ) experiment is in progress. We investigate levels of ^{113}Cd by the (d,p) reaction at the Munich Tandem Accelerator at the Q3D spectrograph. ^{112}Cd targets with an enrichment of 99% were bombarded by 20 MeV deuterons. Spectra were recorded at 20, 40 and 60 degrees. The spectrum with an energy resolution of 6-7 keV recorded at 20 degree is shown in Fig. 1.

Below 1 MeV we observe all J$\leq$11/2 spin states known from the literature. We aim to extend the level scheme up to ca. 2.5 MeV and to extract L-transfer values and single-particle strengths for states which have not been sufficiently resolved in [5].

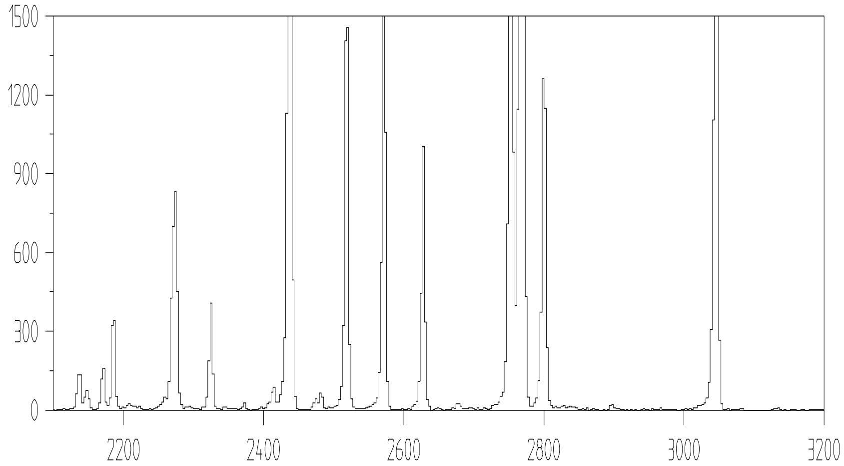

Fig. 1: Part of the ^{112}Cd(d,p)^{113}Cd spectrum at E_d = 20 MeV for E_x up to 1.150 MeV at 20 degree scattering angle.

[1] Zs. Németh et al., Proc. Int. Conf. on Nuclear Astrophysics: 'Nuclei in the Cosmos', Karlsruhe, 1992. F. Käppeler, editor (Institute of Physics, Bristol, 1993) in press
[2] Th. Kröll, Thesis, Universität Frankfurt (1991).
[3] Zs. Németh et al., Bull. Am. Phys. Soc. 37, 937 (1992).
[4] W. Geiger et al., Verh. Deutsch. Phys. Ges. 28, 582 (1993).
[5] L. H. Goldman, J. Kremenek and S. Hinds, Phys. Rev. 179, 1172 (1969).

2.1.6 Excitation of ^{144}Sm in (p,p') and (α,α')

E. Müller-Zanotti, R. Hertenberger, B. Valnion, W. Oelmaier, D. Hofer, G. Graw,
Gh. Cata-Danil [a], G. Lazzari [b], P.F. Bortignon [c]
[a] Institute of Atomic Physics, Bucharest, Romania
[b] Dipartimento di Fisica dell'Universita, Milano, Italy

The excitation of ^{144}Sm has been studied in (p,p') with an energy resolution of 4-5 keV using 22 MeV protons and with 40 MeV alphas, (α, α') with a resolution of 12 keV. Fig. 1 shows a spectrum of the (α, α') reaction.

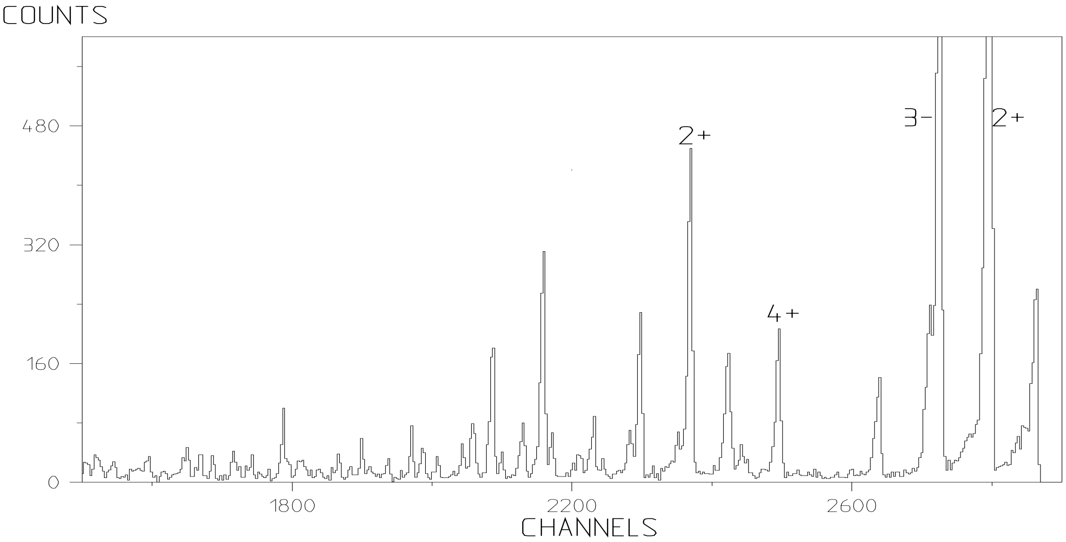

Fig. 1: ^{144}Sm (α, α'), $\theta = 20^0$, $E_\alpha = 40 MeV$.

The (p,p') angular distributions for states up to 4 MeV excitation energy are compared with distorted-wave and coupled-channels calculations including one-step and two-step excitations to study direct and sequential strength distributions [1]. The results are compared with calculations in the nuclear field theory (NFT) approach where QRPA like states [3], two-phonon (quadrupole and octupole) states and their mixing are taken into account. Reasonable agreement is obtained both for the positive and the negative parity states.

In the (p,p') analysis we use the knowledge about excitation energies and quantum numbers from [2] and the present high resolution (p, p') scattering results to derive information about direct and sequential transition probabilities. We furthermore include the information about enhanced E1 transition strengths from [2] to compare with these NFT calculations.

These calculations successfully reproduce the main features of the data: the number of states and the distribution of direct excitation strength for the different quantum numbers.

For the negative parity quadrupole-octupole two–phonon quintuplet the excitation energies and for the 1^-, 2^- and 3^- states of this multiplet the observed E1 decay strength are reproduced nicely, fig. 2. For the positive parity candidates of two–phonon excitation of the quadrupole-quadrupole and octupole-octupole type the calculations predict considerable spreading of the E1 transition strength and the observed order of magnitude for the few observed states, fig. 3. In (p,p') all two-phonon candidates are observed, the cross section angular distributions deviate in part from calculations for pure two–phonon states but remain within the predicted order of magnitude.

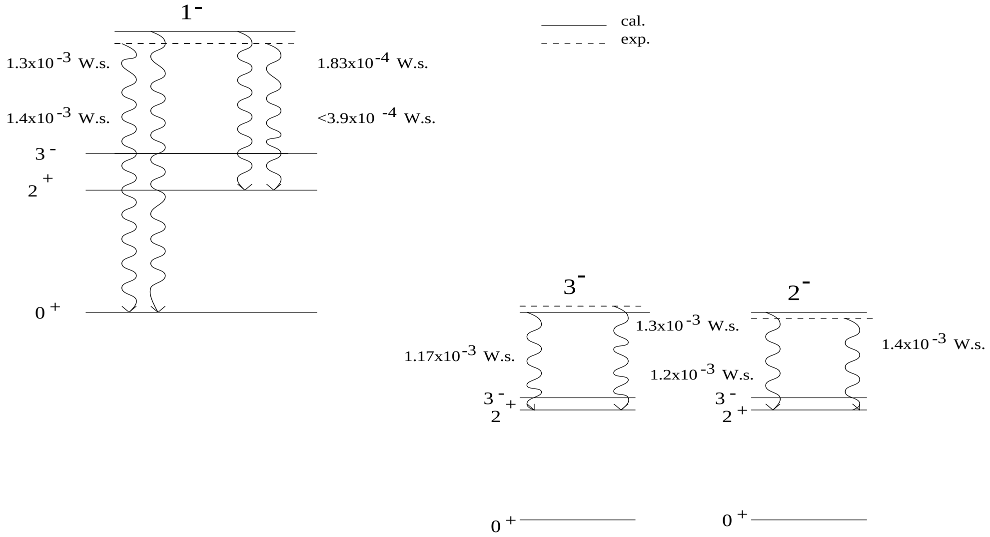

Fig. 2: Partial level scheme and the calculated transition rates for $1^-, 2^-$ and 3^- members of the quadrupole–octupole quintuplet.

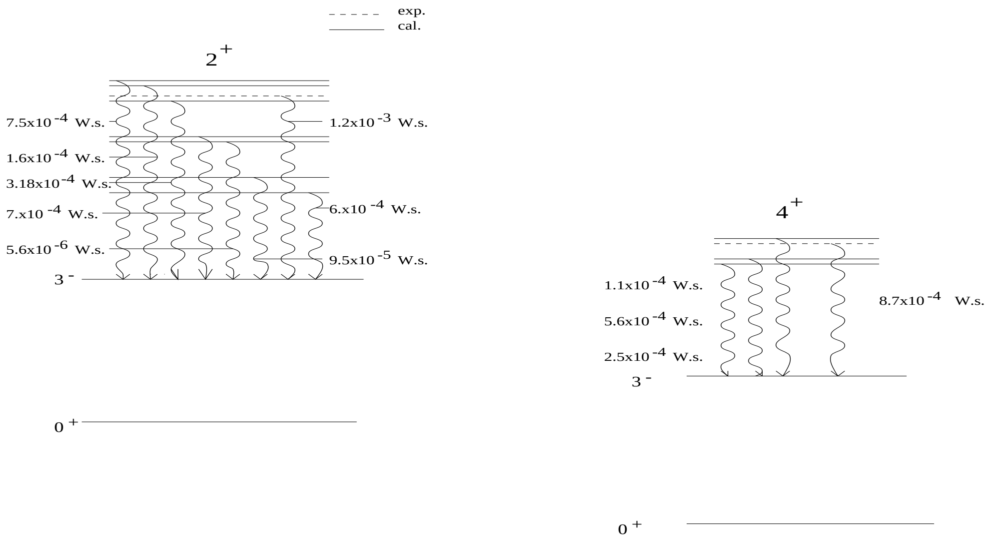

Fig. 3: Partial level scheme and the calculated transition rates for 2^+ and 4^+ states.

Some mixing of two–phonon strength with two–quasiparticle direct excitation strength apparently is affecting the observed inelastic scattering angular distributions.

The study with alpha particles is expected to give more detailed information on the collective behavior on enhancement of sequential excitations. This study is still in work.

[1] E.Müller–Zanotti et al., accepted in Phys. Rev. C
[2] R.A.Gatenby et al,Phys.Rev.C41 (1990),R414
[3] Broglia, P.F.Bortignon, Milano, priv.comm.(1992)
[4] E.Zanotti, Thesis, LMU Muenchen (1991)

2.1.7 The influence of transfer on subbarrier fusion

Th. Winkelmann, F.J. Schindler, K. Balog, T. Beha, P. Jänker, Th. Kerscher, H. Leitz, K.E.G. Löbner, M. Moralles, K. Rudolph, H.-G. Thies

In recent years, there has been an increasing interest to study heavy-ion reactions around the Coulomb-barrier. This interest is caused mainly by the observation of enhancement of several orders of magnitude in the subbarrier fusion cross sections compared to predictions based on tunnelling through a one-dimensional barrier. In addition unexpected variations were found for the subbarrier fusion cross section of neighbouring isotopes [1].

The aim of our experiments was to analyze the influence of one and more-particle transfer on the fusion enhancement. Therefore, measurements of the systems $^{32}S \longrightarrow {}^{92,98,100}Mo$ (at the barrier and 5 MeV below the barrier) and $^{32}S \longrightarrow {}^{102,104}Ru$ (at the barrier) have been performed. The angular distributions of the transfer cross sections have been compared with semiclassical calculations in first order perturbation theory. One nucleon transfer is well described, but multi-nucleon transfer experiments show a lack of cross section for higher angles (= closer distances) relative to the theoretical values (Fig. 1). One possible description of this phenomenon is that the missing flux goes into fusion and leads to the observed enhancement of subbarrier fusion [2].

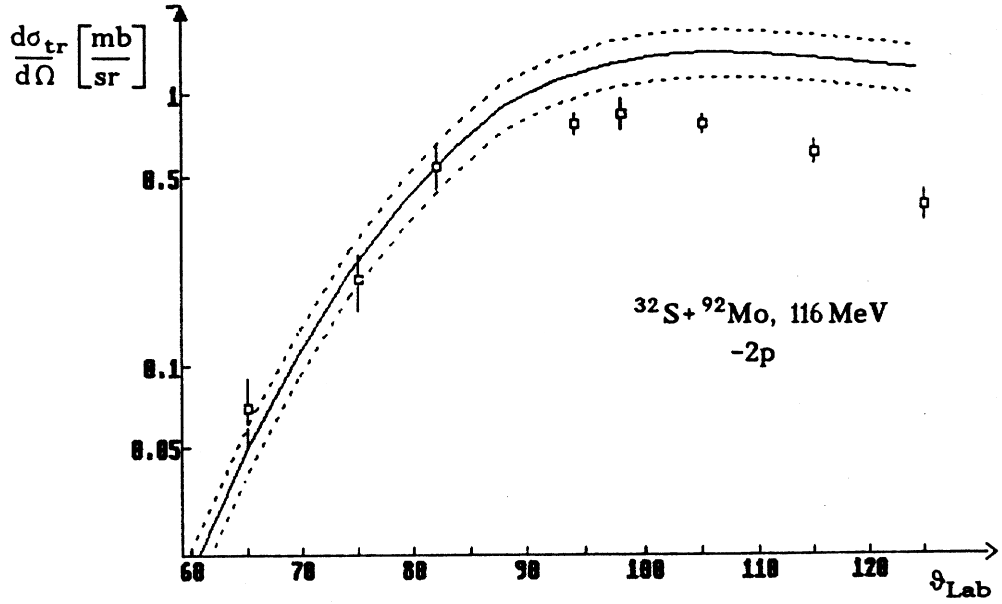

Fig. 1: Comparison of measured angular distribution of the cross section for the $^{92}Mo(^{32}S,^{30}Si)^{94}Ru$ reaction. Full curve: Semiclassical calculation. Dotted curves: Variation of the formfactor strength ±20 %.

One can also determine the strength of the formfactors from the forward part of the angular distributions. This allows a calculation of the fusion cross section in a coupled channel formalism [3]. It can be seen (Fig. 2) that the transfer channels play an important role. Coupling to the inelastic channels alone can not explain the large enhancement of subbarrier fusion. Also the isotopic variations can be well explained including transfer reactions. Another important feature which can be obtained from coupled channel calculations based on the experimental values of the formfactors is the average angular momentum of the compound nucleus produced in the fusion process. Figure 3 shows a good agreement with measured angular momenta [4].

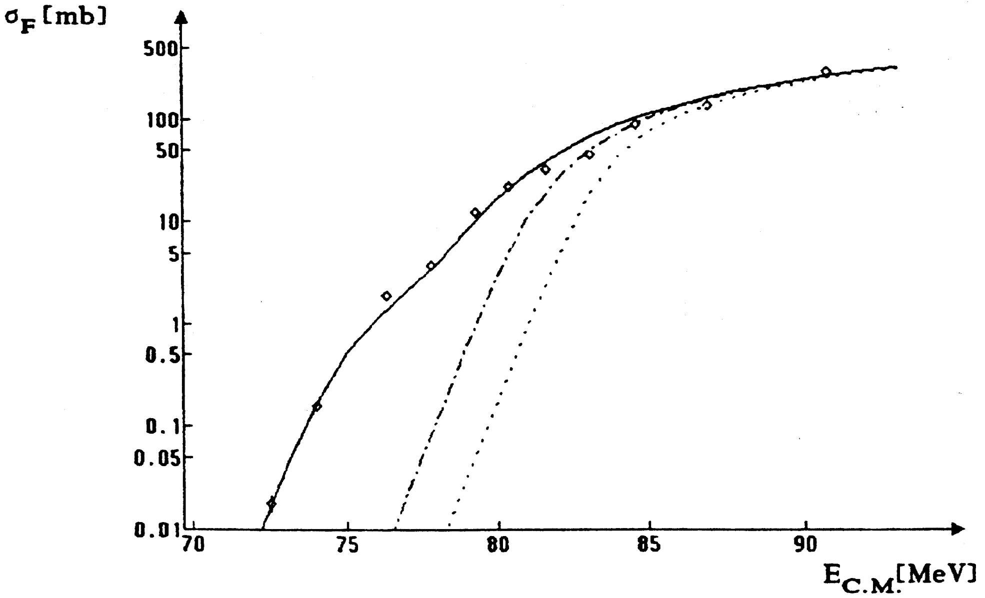

Fig. 2: Fusion excitation function of the reaction $^{32}S \longrightarrow {}^{100}Mo$. Dotted curve: One-dimensional tunnelling. Dashed dotted curve: Coupled channels calculation with inelastic channels only. Full curve: Coupled channels calculation with inelastic and transfer channels. Measured points are from [5].

There are still some questions left, e.g. the estimated formfactors show an energy dependence which can not be understood in the semiclassical picture we have used. Another problem is the impossibility to distinguish between elastic and quasi-elastic channels in the experiment. Experiments to clear up this questions are in progress.

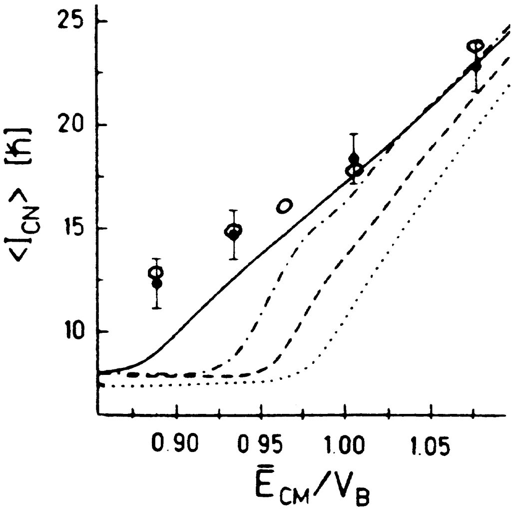

Fig. 3: Average angular momentum in fusion of ^{32}S + ^{100}Mo versus the energy relative to the barrier measured by Hennrich et al. [4]. Full circles: Measured values. Open circles: Our calculation based on our transfer measurement. Curves: Several model calculations discussed in [4].

[1] M. Beckerman et al., Phys. Rev. Lett. **45** (1980) 1472
[2] L. Corradi et al., Z. Phys. **A334** (1990) 55
[3] C.H. Dasso, S. Landowne, Nucl. Phys. **A405** (1983) 381
[4] H.-J. Hennrich et al., Phys. Lett. **B258** (1991) 275
[5] R. Pengo et al., Nucl. Phys. **A411** (1983) 255

2.1.8 Cross sections for Coulomb excitation of a 2.8 MeV state in ^{180}Ta and for the one-neutron pickup reaction ^{181}Ta(^{32}S,^{33}S)^{180}Ta

J. de Boer, C.H. Dasso [a], P. von Neumann-Cosel [b], A. Richter [b], C. Schlegel [b]
[a] Niels Bohr Institute, Copenhagen, Denmark
[b] Technische Universität Darmstadt

Photoabsorption experiments performed at the DANILAC facility suggest that a transition from the 75.3 keV 10^{15}y isomeric 9^- state in ^{180}Ta to an intermediate state of about 2.8 MeV excitation energy can lead to a population of the ground state which β^--decays to ^{180}Hf. Attempts are being made to determine the excitation energy of and the matrix element to this intermediate state by Coulomb excitation with ^{32}S ions. The extremely low natural abundance (0.01%) of ^{180}Ta as compared to ^{181}Ta makes it possible for the one-neutron pickup ^{181}Ta(^{32}S,^{33}S)^{180}Ta to compete when natural targets are used.

Results of model calculations for the two projectiles ^{32}S and ^{36}S are shown in Figs. 1 and 2. They may provide guidelines for the range of bombarding energies in which the Coulomb excitation of the isomeric state dominates the population of the ^{180}Ta ground state whose 8 h β^--decay is used to determine its population out of beam.

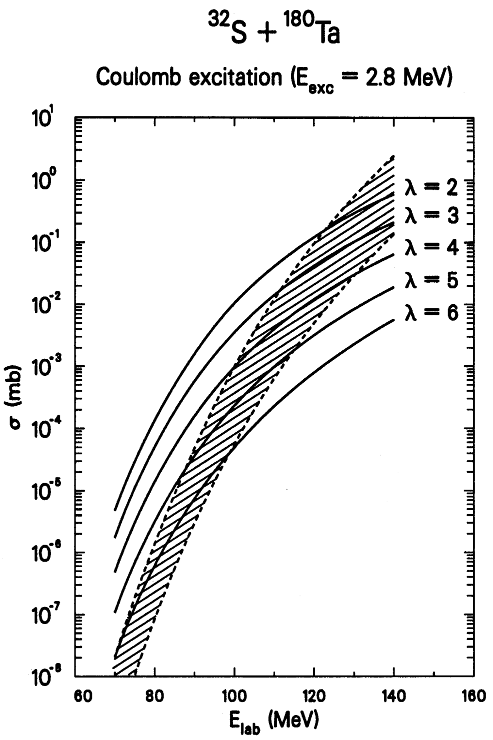

Fig. 1: Total Coulomb excitation cross-section by different multipolarities λ for the excitation of a 2.8 MeV state in ^{180}Ta by ^{32}S projectiles. The matrix elements used in the calculation all have values $0.5\,e \cdot (10\mathrm{fm})^{\lambda}$. The shaded area indicates the range of the cross section expected for the ^{181}Ta(^{32}S,^{33}S)^{180}Ta pickup reaction

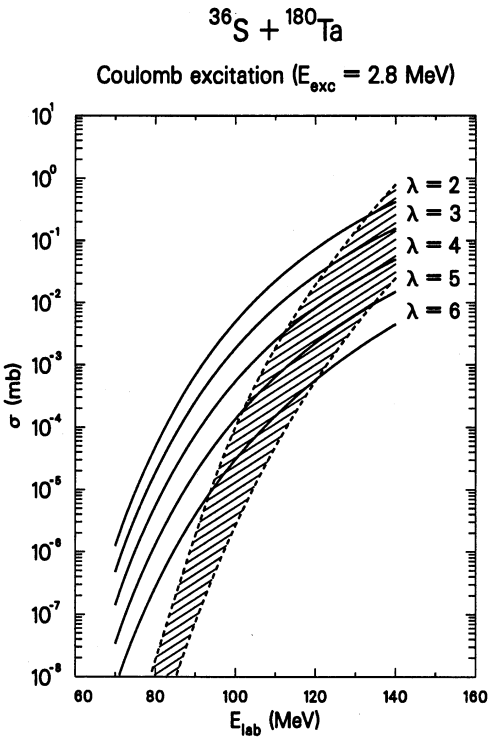

Fig. 2: Total Coulomb excitation cross-section by different multipolarities λ for the excitation of a 2.8 MeV state in ^{180}Ta by ^{36}S projectiles. The matrix elements used in the calculation all have values $0.5\,e \cdot (10\mathrm{fm})^{\lambda}$. The shaded area indicates the range of the cross section expected for the ^{181}Ta(^{36}S,^{37}S)^{180}Ta pickup reaction

2.1.9 Coulomb excitation of ^{231}Pa with ^{16}O and ^{32}S

M. Springer, J. de Boer, A. Gollwitzer, N.A. Gollwitzer, A. Lösch, F. Rieß, E.G. Vogt, M. Würkner

A radioactive target of 133 μg/cm^2 ^{231}Pa was bombarded with 145 MeV ^{32}S and with 85 MeV ^{16}O projectiles. The gamma-rays were measured by five Compton-suppressed high-purity germanium counters in coincidence with the backscattered projectiles, which were detected in an array of 24 PIN-diodes.

In a former experiment with 140 MeV ^{32}S projectiles some strong lines could not be assigned (128 keV, 140 keV, 218 keV) and the experimental intensities for the transitions in the negative signature branch differ from those calculated using rotational values for the electromagnetic matrix elements [1] [2]. The measurements presented here served to check the ^{32}S experiment (performed with Li-drifted Ge counters) an to obtain additional confirmation of observed Coulomb-excitation induced gamma lines in a bombardment with oxygen ions. The unassigned lines are again observed in both new experiments and are thus shown to belong to the decay of Coulomb excited levels of ^{231}Pa.

The observed gamma intensities are compared with calculations using the rotational parameter $Q_0 = 9.2$ b for the E2 and $g_k = 2.8$, $g_R = 0.4$, b =1.22 for the M1 matrix elements. The lines marked by ? are proposed to belong to transitions from the 1/2[530] ground-state band to a positive-parity band consisting of strongly octupole mixed 3/2[651] and 3/2[521] Nilson orbitals [3]. A detailed evaluation is in progress.

[1] J. de Boer et al. In-beam spectroscopy of ^{231}Pa, Zeitschrift für Physik A - Hadrons and Nuclei, 1992, 344, p. 41 - 48

[2] J. de Boer et al. The Rotational Bands in the Nuclei ^{229}Pa and ^{231}Pa, Prog. Part. Nucl. Phyis., 1992, A28, p. 429 - 434

[3] J. Kvasil, J. de Boer, N. Gollwitzer, A. Lösch. The microscopic structure of low-lying states in ^{229}Pa and ^{231}Pa, Verhandl. DPG (VI)28, 609, 1993

E_γ (keV)	Intensity this work	Intensity Ref. [1] [2]	$\frac{I_\gamma(exp)}{I_\gamma(Coulex)}$	Assignement
58.4	3.37	8.7	0.42	$7/2^- \rightarrow 3/2^-$
69.0	0.80		2.65	$5/2^- \rightarrow 1/2^-$
110.5	100	100	1.00	$11/2^- \rightarrow 7/2^-$
115.9	2.48	2.9	1.49	$9/2^- \rightarrow 5/2^-$
128.0	2.34	1.8		$19/2^- \rightarrow 17/2^+$?
140.0	28.4	23		$15/2^- \rightarrow 13/2^+$?
160.3	152	123	1.18	$15/2^- \rightarrow 11/2^-$
200.0	13.1		2.31	$17/2^- \rightarrow 13/2^-$
207.0	50.0	32	1.23	$19/2^- \rightarrow 15/2^-$
218.9	16.6	10		?
236.7	6.42	2.8	4.05	$21/2^- \rightarrow 17/2^-$
249.9	11.7	6.6	1.96	$23/2^- \rightarrow 19/2^-$

Table 1: Energies and intensities of assigned transitions in ^{231}Pa excited with 145 MeV ^{32}S . The measured intensities are normalized: I (110.6 keV) = 100 and are compared with calculated values : $\frac{I_\gamma(exp)}{I_\gamma(Coulex)}$(110.6 keV) = 1.00. The Coulomb-excitation calculation used the rigid-rotor model with values Q_0 = 9.2 b, g_k = 2.8, g_R = 0.4, b =1.22

E_γ (keV)	Intensity	$\frac{I_\gamma(exp)}{I_\gamma(Coulex)}$	Assignement
59.0	4.68	0.38	$7/2^- \rightarrow 3/2^-$
68.7	0.22	0.39	$5/2^- \rightarrow 1/2^-$
110.5	100	1.00	$11/2^- \rightarrow 7/2^-$
116.0	2.80	1.74	$9/2^- \rightarrow 5/2^-$
129.0	1.72		$19/2^- \rightarrow 17/2^+$?
140,0	17.4		$15/2^- \rightarrow 13/2^+$?
160.3	90.6	1.28	$15/2^- \rightarrow 11/2^-$
199.8	4.49	2.92	$17/2^- \rightarrow 13/2^-$
206.9	18.6	1.51	$19/2^- \rightarrow 15/2^-$
218.1	8.78		?
236.5	5.50	22.8	$21/2^- \rightarrow 17/2^-$
249.8	6.40	6.3	$23/2^- \rightarrow 19/2^-$

Table 2: Energies and intensities of assigned transitions in ^{231}Pa excited with 85 MeV ^{16}O. The measured intensities are normalized: I (110.6 keV) = 100, the measured intensities are compared with calculated values : $\frac{I_\gamma(exp)}{I_\gamma(Coulex)}$(110.6 keV) = 1.00. The Coulomb-excitation calculation used the rigid-rotor model with values Q_0 = 9.2 b, g_k = 2.8, g_R = 0.4, b =1.22

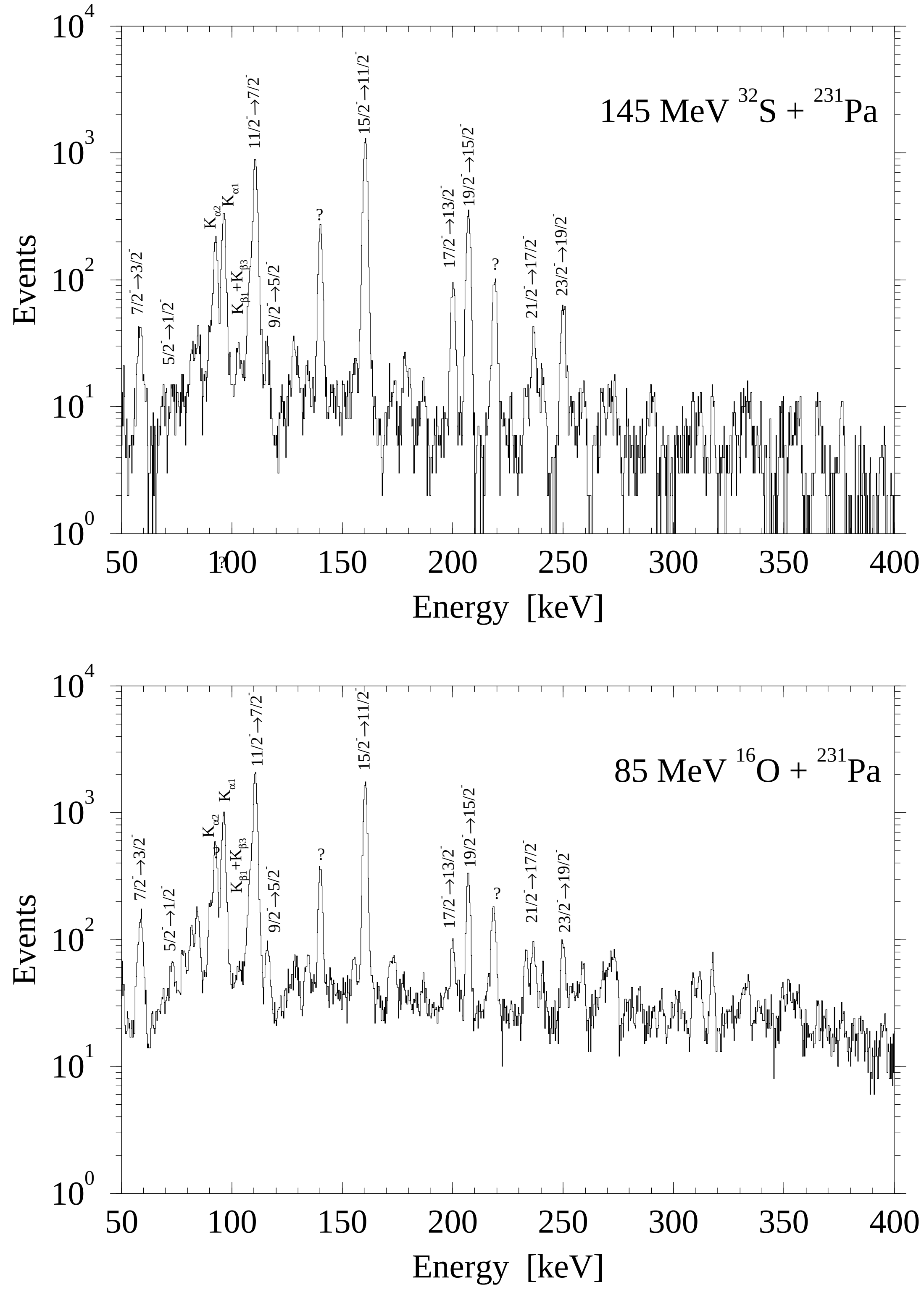

Fig. 1: Gamma-spectra of Coulomb-excited ^{231}Pa in coincidence with backscattered 145 MeV ^{32}S (above) and 85 MeV ^{16}O (below).

2.1.10 Projectile fragmentation of Xe ions at E_{lab}=790 A·MeV

J. Friese, H.-J. Körner, J. Reinhold, R. Schneider, K. Zeitelhack
H. Geissel [a], A. Magel [a], G. Münzenberg [a], K. Sümmerer [a]
[a] Gesellschaft für Schwerionenforschung, Darmstadt

In 1992 we investigated the production of heavy neutron rich and neutron deficient nuclei by fragmentation of ^{129}Xe projectiles impinging on a 803 mg/cm^2 ^{27}Al target at E_{kin} = 790 A·MeV. The experiment was performed at the magnetic spectrometer Fragmentseparator FRS [1] at GSI Darmstadt.

A multilayer array of silicon detectors was mounted in the intermediate dispersive focal plane of the FRS to measure the position ($\Rightarrow B\rho$) and energy loss ($\Rightarrow$ nuclear charge Z) of the fragments. The velocity was measured with a RICH (Ring Imaging Cherenkov) detector [2, 3] mounted at the final FRS focus. The obtained resolutions of ΔA=0.67(fwhm) and ΔZ=0.43(fwhm) allow unambiguous fragment identification.

Production cross sections from 30 mbarn down to 1 nbarn were determined for nuclei in the mass region 80<A<129. In fig. 1 measured cross sections for three isotopic chains are compared to an empirical parameterization based on target fragmentation data (EPAX[4]) and to an abrasion ablation model (ABRABLA[5]).

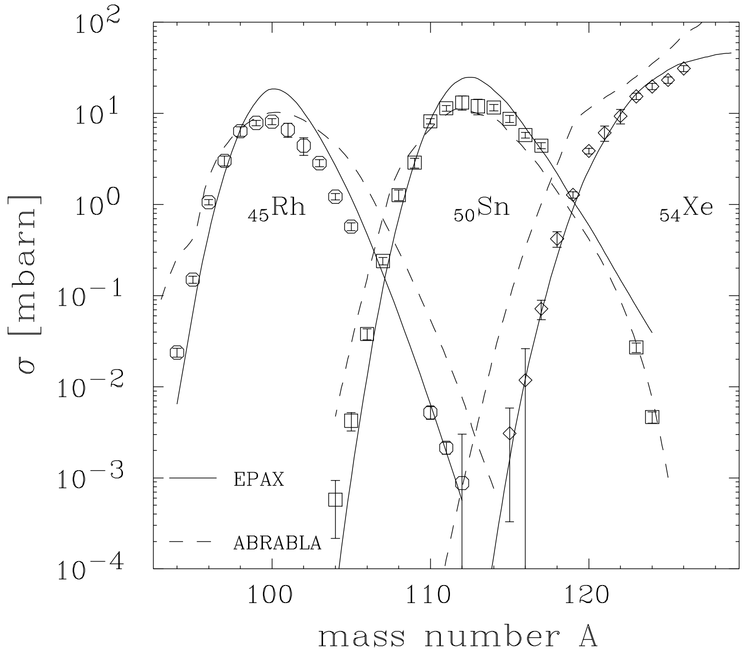

Fig. 1: Measured isotopical distributions for a subset of 3 sample elements compared to EPAX (full line) and ABRABLA (dashed line).

The maxima of the distributions are well predicted in position by EPAX, but the absolute values are overestimated by a factor of about two. The neutron deficient side is in good agreement for the Xe fragments but slightly underestimated for isotopes with lower nuclear charge. The large deviations for the neutron rich Sn fragments were also seen in earlier experiments with a ^{136}Xe beam [2, 6, 7]. This is due to an inherent overestimation by EPAX for the widths of the charge dispersions of isobaric chains very close to the projectile.

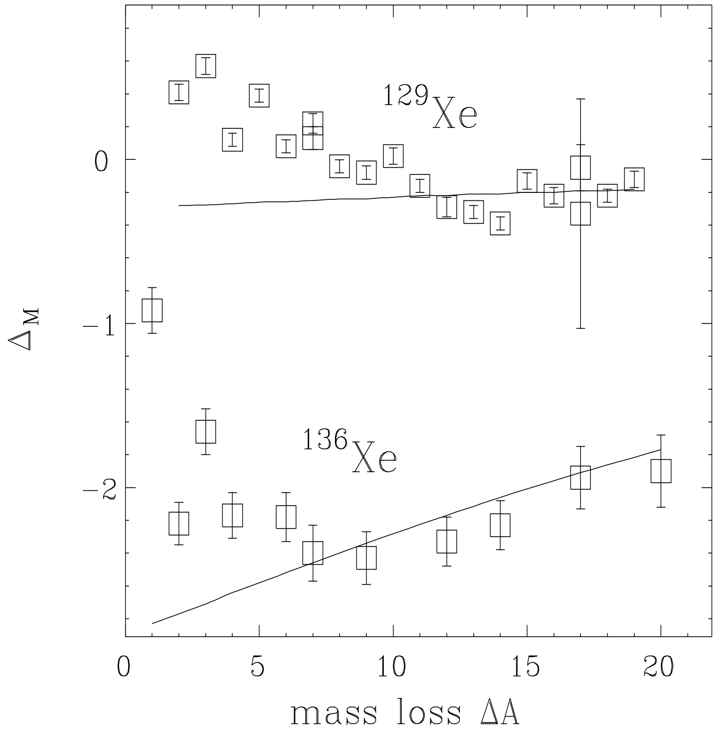

Fig. 2: Memory effect parameter Δ_M extracted from our data in comparison to the EPAX prediction (full line).

ABRABLA uses a statistical abrasion model followed by a macroscopic evaporation code. An excitation energy of 13 MeV was assumed for each nucleon removed in the abrasion stage. For the neutron deficient Xe isotopes the calculated distribution disagrees up to one order in magnitude. The neutron rich side is well described for nuclear charges near the projectile. With decreasing proton number the predicted distributions are too broad.

The two xenon projectiles, ^{129}Xe and ^{136}Xe, used in the present study and that of ref. [7] have sufficiently different A/Z ratios to allow a comparison with the EPAX prediction of the "memory effect", i.e. the influence of the projectile A/Z ratio on the corresponding fragment yield (see ref. [4] for details). In fig. 2 we compare the experimental memory effect parameter Δ_M deduced from our data to the EPAX predictions. The substantial difference between the two systems is well reflected by the EPAX parameterization. The large memory effect observed for ^{136}Xe fragments with mass losses as large as 20 mass units is indicative of a large contribution of abrasion-like mechanisms in the formation of the respective fragments.

Longitudinal momentum transfers were measured with good accuracy ($\Delta P/P < 10^{-3}$) for all produced isotopes. They are compared to empirical systematics [8] by using the quantity

$$\langle \tilde{P} \rangle \equiv M_{proj} \cdot \langle \beta_{proj.fr.} \rangle \cdot c \cdot k,$$

where M_{proj} is the projectile mass , $\langle \beta_{proj.fr.} \rangle$ the mean velocity of the fragment in the projectiles rest frame and $k = (\gamma - 1)/(\beta \cdot \gamma)$ a kinematic factor, which approaches 1 for large kinetic energies of the projectile. If one neglects the mass loss in the first reaction step $M_{proj} \cdot \langle \beta_{proj.fr.} \rangle$ is the momentum transfer to the prefragment in the projectiles rest frame. Thus $\langle \tilde{P} \rangle$ could be connected to the prefragment

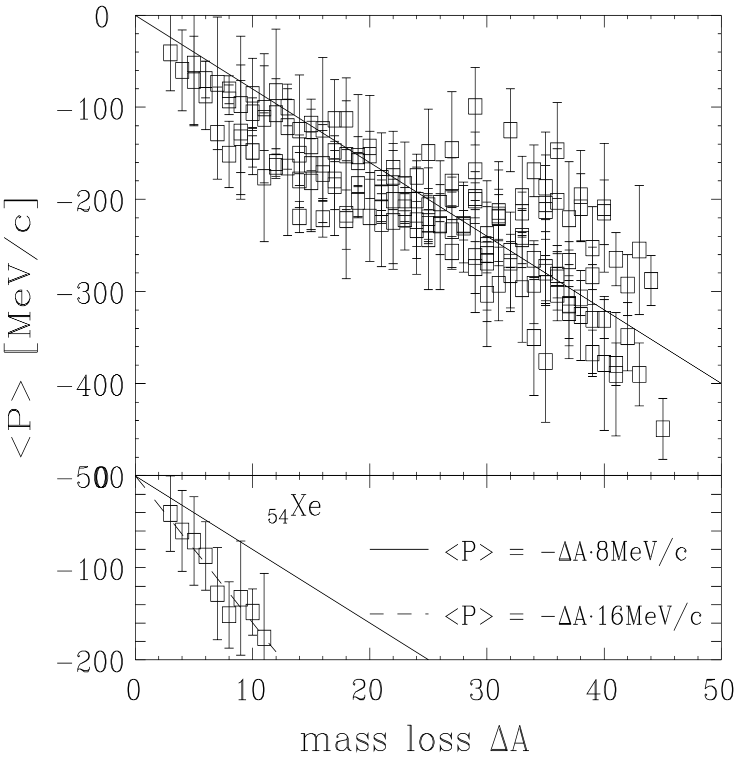

Fig. 3: Mean momenta of projectile fragments in the projectile rest frame. Top: all measured isobars. Bottom: same for Xe isotopes. Full line: systematics according to [8]. Dashed line: best fit to the Xe data.

excitation energy via the relation $E_{kin} = pc \cdot k$. For fragments with a constant mass to charge ratio the data show on the avarage the expected trend [8] of roughly $\langle\tilde{P}\rangle = -\Delta A \cdot 8MeV/c$ (fig. 3). However, a momentum downshift twice as large was observed for Xe fragments as shown in the bottom part of fig. 3.

[1] H. Geissel et al., Nucl. Instr. Meth. A 70, 286, 1992
[2] K. Zeitelhack, GSI-92-25 Report November 1992
[3] K. Zeitelhack et al., submitted to Nucl. Instr. Meth. A
[4] K. Sümmerer et al., Phys. Rev. C 42 (1990) 2546
[5] J.-J. Gaimard and K.-H. Schmidt, Nuclear Physics A 531 (1991) 709
[6] K.-H. Schmidt et al., Nuclear Physics A 542 (1992) 699
[7] J. Friese et al., Proc. of the International Nuclear Physics Conference, Wiesbaden 1992, to be published in Nuclear Physics A
[8] D.J. Morrissey, Phys. Rev. C 39 (1989) 460

2.1.11 Subthreshold antiproton production in Ne and Ni induced reactions

A. Gillitzer, J. Homolka, P. Kienle, F. Schumacher,
A. Schröter [a], W. Koenig [a], E. Berdermann [a], H. Ströher [b], B. Povh [c]
[a] GSI Darmstadt
[b] Universität Gießen
[c] MPI Heidelberg

We continued our investigation of antiproton ($\overline{p}$) and negative kaon (K^-) and pion (pi^-) creation in relativistic heavy ion collisions at the heavy ion synchrotron SIS at GSI. The maximum beam energy of $2\,GeV/$u is far below the $\overline{p}$ production threshold in a free nucleon nucleon collision of $5.6\,GeV/$u, and also below the K^- production threshold of $2.5\,GeV/$u. If the Fermi momenta of the projectile and target nucleons are included, the $\overline{p}$ threshold is still $\sim 3\,GeV/$u. Therefore antiproton production at these energies is only possible in multistep processes, involving nucleon resonances Δ and $N^\star$, which play an important role as a reservoir of additional available energy.

Using the experimental setup and methods described in [1, 2, 3] we focused Ni ions with energies of 1.8 and $1.9\,GeV/$u on Ni targets. Besides a target of $\sim$ 18 mm thickness optimized for maximum antiproton yield a $\sim$9 mm target was used to investigate the corrections due to target thicknesses which are in the order of the interaction length.

Production cross sections for antiprotons were measured at momenta of 1.5 and $1.9\,GeV/$c, corresponding to center of mass kinetic energies of approximately 60 MeV and 150 MeV. K^- were measured from $1.0\,GeV/$c to $2.2\,GeV/$c and π^- from $0.5\,GeV/$c to $2.8\,GeV/$c.

The antiproton yield obtained in the Ni + Ni experiment was considerably lower ($\sim$ 0.3–0.5 $\overline{p}$/h) than in the Ne + NaF or Ne + Sn reaction ($\sim 1-2$ $\overline{p}$/h), since the maximum beam intensity was lower ($3*10^8$ Ni ions/spill compared to $2*10^9$ Ne ions/spill).

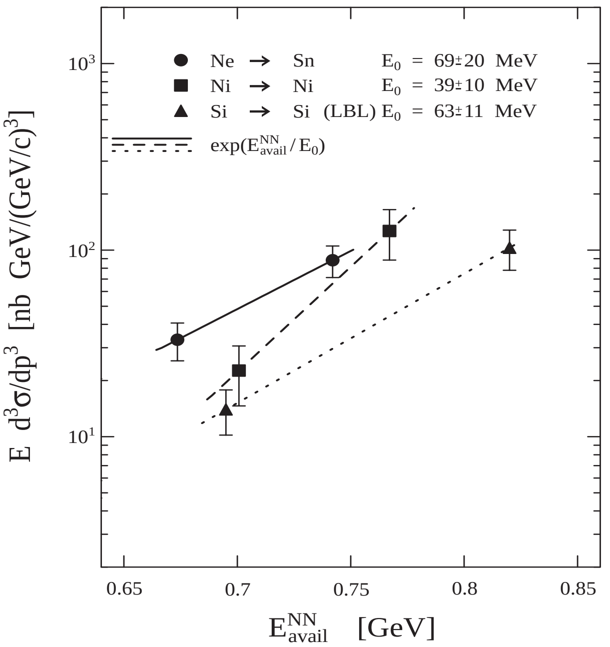

Fig. 1: Excitation functions for subthreshold $\overline{p}$ production in Ne + Sn, Ni + Ni and Si + Si collisions. E_0 are the slope parameters (see text).

Fig. 1 shows the invariant $\overline{p}$ production cross sections measured for Ne + Sn and Ni + Ni versus the mean available kinetic energy E^{NN}_{avail} in a nucleon nucleon collision inside the collision zone. E^{NN}_{avail} depends on the beam energy and the ratio of projectile and target participant sizes. For comparison the Berkeley data for Si + Si are included [4].

The Ne + Sn and Si + Si cross sections can be described by exponential curves ($\sigma \sim \exp{(E^{NN}_{avail}/E_0)}$) with similar slope parameters (Ne + Sn: $E_0 = 70\,\mathrm{MeV}$, Si + Si: $E_0 = 63\,\mathrm{MeV}$). Since the mean number of nucleons involved in a Ne + Sn collision is larger than the one for Si + Si, it is not surprising that the $\overline{p}$ production cross section for a given available energy per nucleon nucleon collision is higher in the first case. For the Ni + Ni system the data suggest a steeper increase of the $\overline{p}$ yield with the mean available kinetic energy ($E_0 = 39\,\mathrm{MeV}$), but within the errors the slope parameters for the Ne + Sn and Ni + Ni reactions could still be the same. A steeper excitation function for Ni + Ni would be an astonishing result, since the number of participating nucleons in this system is larger than in the Ne + Sn system, and a possible enhancement of $\overline{p}$ production at lower energies should increase with the number of involved nucleons.

In the earlier measurements [1, 2, 3] for Ne + NaF, Cu, Sn, Bi a universal scaling law was found for the invariant production cross section of all particles (π^-, K^-, $\overline{p}$) $\sigma_{inv} \propto exp[(E^{NN}_{avail} - E_{prod})/E_0]$, where $E_0 \approx 80\,\mathrm{MeV}$ and E_{prod} is the energy necessary to produce a π^-, K^+K^- or $p\overline{p}$ pair, respectively, plus the kinetic energy of the detected particle in the CM system. This behaviour is shown in fig. 2 (left).

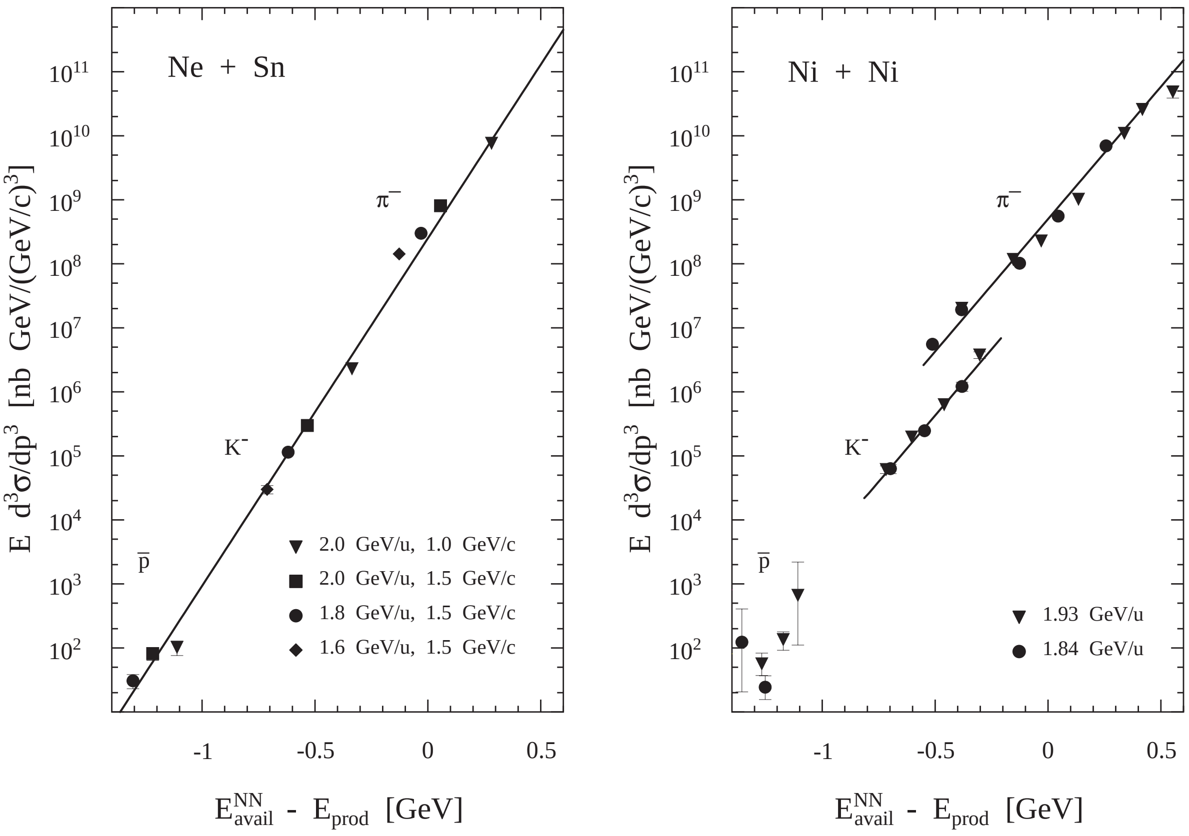

Fig. 2: Production cross sections for $\overline{p}$, K^- and π^- in Ne + Sn (left) and Ni + Ni (right) collisions versus the difference of the mean available energy in a nucleon nucleon collision and the energy required for the particle production (see text).

The slope parameter E_0 then has a twofold significance: For given particle species and energy (fixed E_{prod}) it determines the excitation function, and for fixed available energy E^{NN}_{avail} it describes the kinetic energy distribution of the particles and hence the temperature of the system.

In order to test this simple picture for the Ni + Ni system, a wider range of K^- and π^- momenta was covered to achieve an overlap in the $(E^{NN}_{avail} - E_{prod})$ regimes of the two particle species. As the comparison in fig. 2 shows, one cannot describe the Ni + Ni data (right) by a single exponential curve as in the Ne + Sn case before. Different exponential curves for pions and kaons are necessary. They are flatter ($E_0^{K^-} = 104\,\mathrm{MeV}$, $E_0^{\pi^-} = 116\,\mathrm{MeV}$) than the universal curve for Ne + Sn ($E_0 = 78\,\mathrm{MeV}$). In order to draw definite conclusions whether there is a different behaviour for the both systems, also the Ne + Sn reaction should be studied with π^- and K^- in the full momentum range between 0.5 and $2.8\,GeV/c$.

A possible explanation for the deviations from the scaling law, observed in the Ni + Ni system, is the momentum dependent absorption of secondary particles inside the collision zone. This would reduce the measured cross sections at low momenta and in this way divide a universal curve in segments with reduced steepness for each particle class.

The momentum dependence of the $\overline{p}$ production cross section is shown explicitely in fig. 3. For all systems the decrease of the $\overline{p}$ yield with increasing momentum is rather weak since the effect of increasing the required energy for the $\overline{p}$ production is nearly counterbalanced by the decreasing absorption cross section.

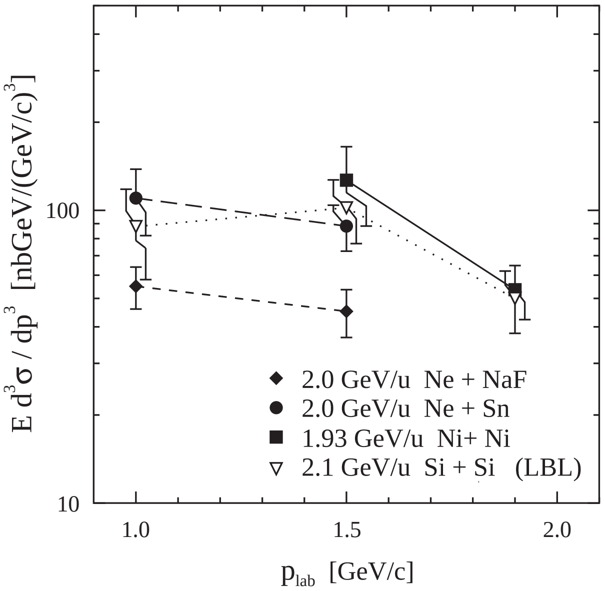

Fig. 3: Momentum dependence of the invariant $\overline{p}$ production cross section. The data for Si + Si are from Ref. [4].

[1] A. Gillitzer et al., Proc. XXX Int. Winter Meeting on Nuclear Physics, Bormio 27.Jan. - 1.Feb. 1992, p.392

[2] A. Gillitzer et al., Jahresbericht 1991, p.14

[3] A. Schröter et al., Int. Nuclear Physics Conference, Wiesbaden 26.Jul. - 1.Aug. 1992, contribution 3.5.16 and A. Schröter et al., Physica Scripta Vol.47 (1993)

[4] A. Shor et al., Phys. Rev. Lett. **63** (1989) 2192.

2.1.12 Antiproton induced nuclear fission

A.S. Iljinov[a], M.V. Mebel[a], H. Daniel, T. von Egidy, F.J. Hartmann, P. Hofmann, Y.S. Kim
[a] Institute for Nuclear Research, Academy of Sciences of Russia, Moscow 117 312, Russia

The antiproton-nucleus ($\bar{\text{p}}$A) annihilation has two stages. Pions produced in the antiproton-nucleon annihilation initiate the first stage, the intranuclear cascade. Subsequently, the highly excited nucleus evaporates particles or undergoes fission during the second slow stage. Fission, being a slow process and taking place at the second stage, gives us a possibility to study the dissipation of energy in antiproton-nucleus annihilation.

We have developed the statistical model of antiproton induced nuclear fission. The fast stage is described by the intranuclear cascade model [1] in this approach. The slow stage is described by the modified evaporation model [2] which takes into account shell effects and their thermal damping in a correct manner. The fission probability is calculated during each step of an evaporation chain with the help of the well-known Bohr-Wheeler expression based on the existence of the saddle point in fission.

In order to describe the dynamics of the descent of the fissioning nucleus from the saddle point to the scission point, when mass and kinetic energy distributions of the fission-fragments from the highly excited nucleus are formed, we use the diffusion model [3] based on the Fokker-Planck equation. It takes into account the dissipative nature of the fission process and thermal and quantum fluctuations. To describe the low-energy fission ($E^* < 50$ MeV), we have included the empirical approximations which take into account the coexistence of symmetric fission and two modes of asymmetric fission. All stages of antiproton-nucleus annihilation are calculated by the Monte Carlo method. A simulated event of the antiproton-nucleus annihilation contains information about all particles emitted in the intranuclear and evaporation cascades before scission, and about evaporation particles emitted after scission, and also about both fission fragments. Therefore the model may be used for calculations of inclusive and exclusive fission cross sections. The model will be described in detail elsewhere [4].

The experimental data [5, 6] on fission of Bi, Th, U nuclei by stopped antiprotons have been analyzed in the framework of this model. The good agreement between theory and experiment (fig. 1) justifies the application of the model for the study of energy dissipation and scission of hot nuclei after antiproton-nucleus annihilation.

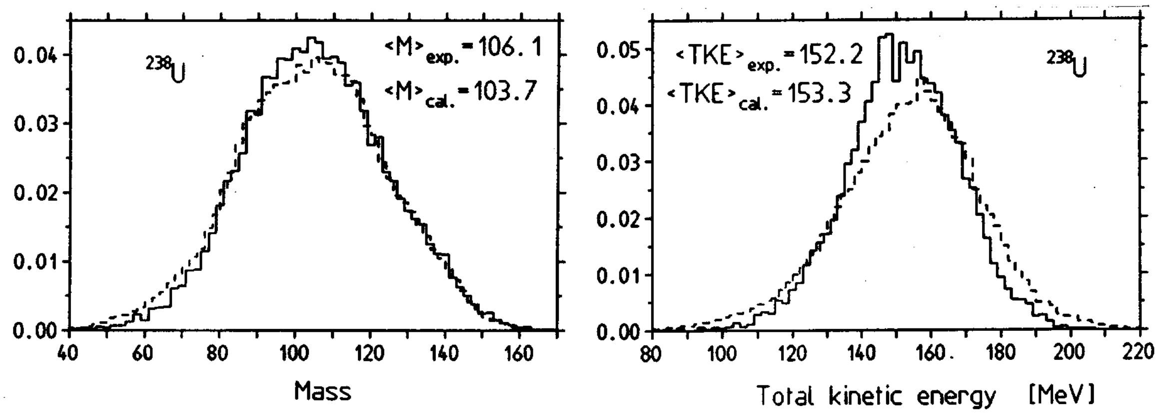

Fig. 1: Mass distribution of fission fragments (left part) and total kinetic energy distribution (right part) in antiproton-nucleus fission. Solid histogram - experiment, dashed histogram - theory. The histograms are normalized to one fission event.

[1] A.S. Iljinov, V.I. Nazaruk, S.E. Chigrinov, Nucl. Phys. **A382** (1982) 378
[2] A.S. Iljinov, M.V. Mebel, N. Bianchi et al., Nucl. Phys. **A543** (1992) 517
[3] G.D. Adeev, I.I. Gonchar, V.V. Pashkevich et al., Particles and Nuclei, **19** (1988) 1229
[4] G.D. Adeev, A.S. Botvina, A.S. Iljinov, M.V. Mebel et al., to be published
[5] Y.S. Kim, Ph.D.thesis TUM, 1992.
[6] P. Hofmann, Ph.D. thesis TUM, 1992

2.1.13 Coincident measurement of particle spectra and fission fragments after antiproton annihilation

W. Schmid, J. Hoffmann, F.J. Hartmann, H. Daniel, T. von Egidy, S. Schmid, D. Hilscher[a], D. Polster[a], H. Rossner[a], K. Knoche[b], A. Grabowska[c], J. Jastrzebski[c], W. Kurcewicz[c], P. Lubinski[c], H. Machner[d], H.S. Plendl[e], S. Neumaier[f], J. Eades[f]
[a] Hahn-Meitner-Institut Berlin, D-1000 Berlin 39, Germany
[b] Universität Hamburg, D-2000 Hamburg 36, Germany
[c] Warsaw University, PL 02-097 Warsaw, Poland
[d] Forschungszentrum Jülich, D-5170 Jülich, Germany
[e] Florida State University, Tallahasse, FL 32306-3016, USA
[f] CERN, CH-1211 Geneva, Switzerland

The interaction and annihilation of antiprotons with nuclei is a very special method to obtain very hot nuclei (E* up to 1 GeV) and nuclei containing strangeness. In contrast to heavy-ion reactions the energy transfer from the annihilation pions does not involve high angular momentum or compression. Antiproton induced fission allows the measurement of several parameters per event and yields detailed information on the fission process and the relevant time scale. The competition between particle emission and fission shows whether fission is a relatively fast or slow process. Recent heavy-ion reactions indicate that fission is relatively slow because most particles are emitted before scission and only few particles are evaporated from the fission fragments [1]. Careful evaluation of the total-mass to total-kinetic-energy correlation of coincident fragments from antiproton induced fission gave a different result, because more particles seem to have been emitted from the fragments than in heavy-ion reactions [2, 3].

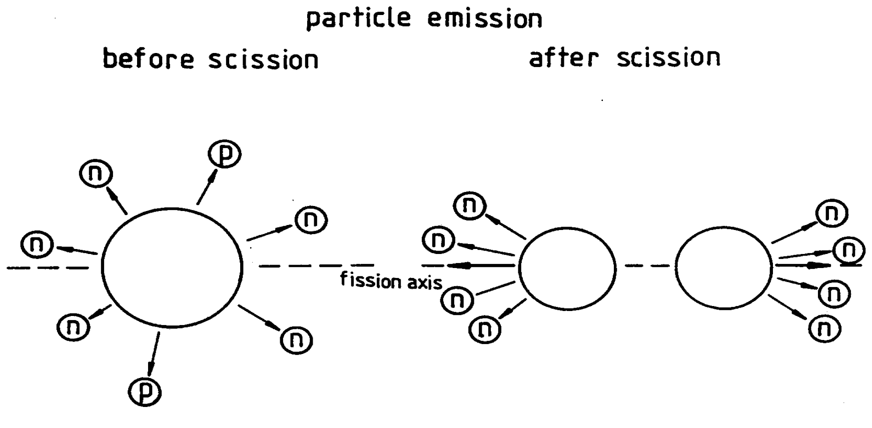

Fig. 1: Distribution of emitted particles before and after scission relative to the fission axis

A new experiment was designed in order to determine the number of particles (mainly neutrons) emitted before and after scission. These particles can be distinguished because particles emitted before scission have an isotropic distribution while particles evaporated from fragments prefer the direction of the fission axis. This is demonstrated in fig. 1. The experimental arrangement is depicted in fig. 2.

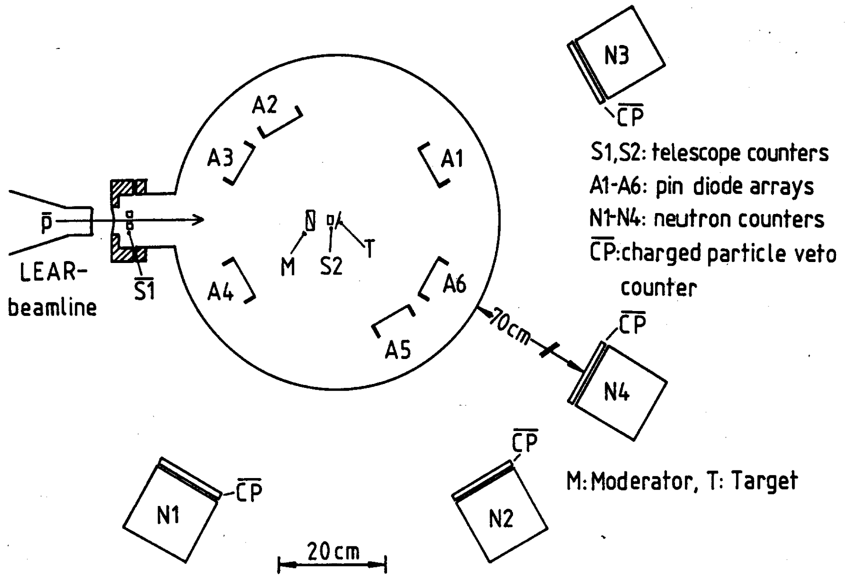

Fig. 2: Fragment spectrometer with particle detectors for antiproton induced fission

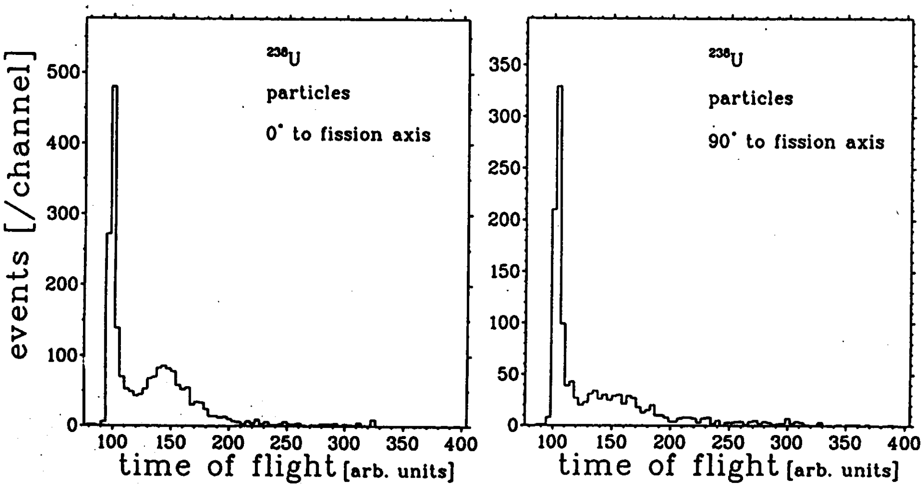

Fig. 3: Time-of-flight spectra of particles emitted parallel and vertical to the fission axis.

The antiprotons are identified with the scintillation counter telescope $\overline{\mathrm{S1}}$S2 and moderated (moderator M) so that they stop in the target T. Energy and time-of-flight of the fragments are measured with pin-diode arrays (A1-A6, each array has 6x12 diodes, and each diode an area of $1\,\mathrm{cm}^2$) which cover 8 % of 4π. Four liquid scintillation counters N1 - N4 determine time-of-flight and energy loss of neutrons and of fast charged particles. These counters are arranged in such a way that they measure particles in parallel and vertical direction to the fission axis given by pairs of opposite pin-diode arrays.

First results are shown in fig. 3. This are time-of-flight spectra of particles in coincidence with two fragments which determine the fission axis. There is a clear increase of particles emitted in parallel direction to the fission axis, indicating particles after scission. The final evaluation of this measurement will shed light on the time scale of antiproton induced fission.

[1] D.J. Hinde, D. Hilscher, H. Rossner, Nucl. Phys. **A502** (1989) 497c.
[2] Y.S. Kim, Ph.D. thesis TUM, 1992
[3] P. Hofmann, Ph.D. thesis TUM, 1992

2.1.14 Inclusive neutral and charged particle spectra from antiproton-nucleus interactions

D. Polster[a], D. Hilscher[a], H. Rossner[a], W. Schmid, P. Baumann, H. Daniel, T. von Egidy, F.J. Hartmann, P. Hofmann, Y.S. Kim, M.S. Lotfranaei
[a] Hahn-Meitner-Institut, D 1000 Berlin 39

The production of hot nuclei by $\bar{\mathrm{p}}$-annihilation in heavy nuclei has become of particular interest in recent years since it provides an alternative method compared to heavy-ion reactions. In the case of antiproton annihilation the intranuclear cascade (INC) model and statistical models have been extensively used to describe energy dissipation until thermalization. Thus it is most interesting to test these models with several observables which are sensitive both to the primary (higher energetic) annihilation process and the various secondary (lower energetic) stages of the thermalization process. For this purpose we have measured simultaneously the energy spectra and multiplicities of $\mathrm{K}^{\pm}$, $\pi^{\pm}$, n, p, d, t over a wide energy range in an experiment at LEAR/CERN [1].

Inclusive energy spectra of neutrons and protons for thick copper and uranium targets are shown in fig. 1. In the case of uranium three sources may be associated with different stages of the energy dissipation in the antiproton-nucleus interaction. The first source represents the fast stage of the intranuclear cascade dominated by sequential two-body collisions of the annihilation pions with nucleons within the nucleus. The intermediate component corresponds to pre-equilibrium emission. Source 3 describes the isotropic evaporation from the compound system (pre-scission neutrons) and the fission fragments (post-scission neutrons) since in this process only slowly moving fragments are expected. No second component was observed in the case of copper because a smaller amount of energy is deposited in this nucleus and the multiplicity of pre-equilibrium neutrons is very low. We have deduced values for the ratio of directly emitted neutrons and protons to be 3.0 ± 0.6 for copper and 3.2 ± 0.5 for uranium. The here presented inclusive neutron-to-proton ratios were measured simultaneously for the first time for two different nuclei. These ratios are sensitive to test especially isospin effects in antiproton-nucleus interactions and their correct consideration in INC models.

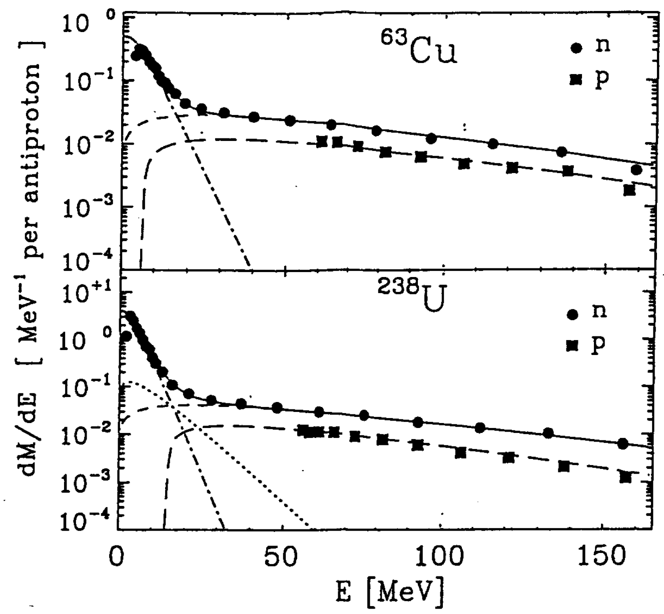

Fig. 1: Energy spectra of neutrons and protons from p̄-annihilation at rest in copper (upper panel) and in uranium (lower panel). The statistical error bars are smaller than the plot symbols. The lines correspond to the different sources (long-dashed lines indicate source 1 for neutrons and protons, short-dashed line source 2 for U, dashed-dotted lines source 3 and solid represent the sum of the different components) for parametrizing the experimental spectra.

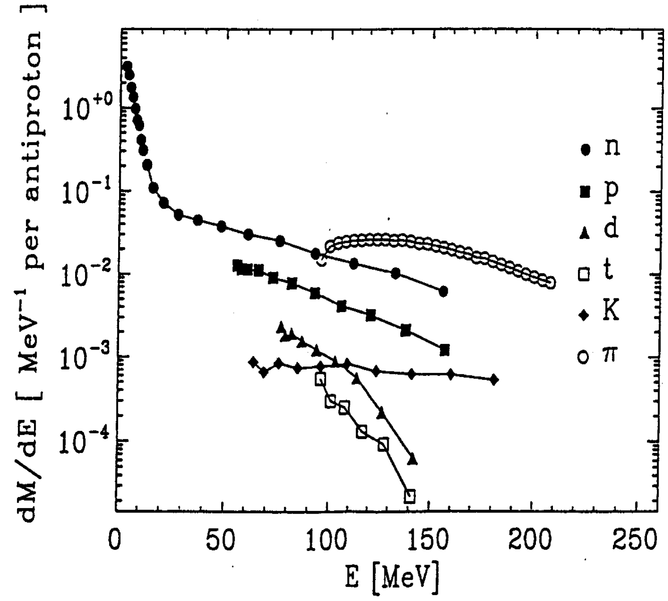

Fig. 2: Energy spectra of all identified particles from q̄-capture in uranium. The data points are connected by lines.

In addition we were able to determine the inclusive spectra of charged mesons. Fig. 2 shows the double differential spectrum of charged kaons together with the n-, p-, t-spectra and for comparison the charged pion spectrum from uranium. The yield of strange particles sheds light especially on the annihilation of the antiproton. If we integrate the kaon spectrum in the measured energy region we find a multiplicity of 0.043 ± 0.013 for $E_{k^\pm} = 64$ to 180 MeV. Using a non relativistic maxwellian-like parametrization with a slope parameter of 128 MeV a value for the total $K^\pm$-multiplicity of 0.125 is obtained.

Recently a further experiment at LEAR was performed to study the dependence of these observables on target masses from C to U. On the basis of these data especially a possible enhanced strangeness production can be discussed.

[1] D. Polster et al., Physics Lett. **B300** (1993) 317

2.1.15 Direct measurement of sticking in muon catalyzed fusion of deuterium-tritium isotopes

D.V. Balin[a], V.N. Baturin[a], P. Baumann, W.H. Breunlich[b], T. Case[c], K.M. Crowe[c], H. Daniel, Yu.S. Grigoriev[a], F.J. Hartmann, A.I. Ilyin[a], M. Jeitler[b], P. Kammel[b], B. Lauss[b], K. Lou[d], E.M. Maev[d], J. Marton[b], M. Mühlbauer, C. Petitjean[c], G.E. Petrov[a], W. Prymas[b], W. Schott, G.G. Semenchuk[a], Yu.V. Smirenin[a], A.A. Vorobyov[a], N.I. Voropaev[a], P. Wojciechowski, J. Zmeskal[b]

[a] Petersburg Nuclear Physics Institute (PNPI), Gatchina 188350, Russia
[b] Austrian Academy of Sciences, Institute for Medium Energy Physics (IMEP),
A-1090 Vienna, Austria
[c] LBL and University of California (UCB), Berkeley, CA 94720, USA
[d] Paul Scherrer Institute (PSI), CH-5232 Villigen PSI, Switzerland

We report new results from our final data runs to determine the sticking parameter ω_s in the muon catalyzed fusion reaction

$$\mathrm{dt}\mu \;\begin{array}{ll} \xrightarrow{1\text{ - }\omega_s}\ {}^4\mathrm{He} + \mathrm{n} + \mu^- & \qquad (1a) \\ \qquad\qquad\qquad + 17.6\ \mathrm{MeV} & \\ \xrightarrow{\omega_s}\ \mu^4\mathrm{He} + \mathrm{n}\ . & \qquad (1b) \end{array}$$

Sticking is a crucial quantity for μCF, since the maximum number of fusions X_c which a muon can catalyze is limited by [1]

$$X_c \leq \frac{1}{\omega_s}. \tag{2}$$

One has to distinguish between "initial" sticking ω_s^o, which is the probability of muon attachment to the ^{4}He-nucleus (α) immediately after dtμ fusion — whereas ω_s defines the "final" sticking probability, after the ${}^4He\mu$-system ($\alpha\mu$) has come to rest. ω_s^o and ω_s differ by the "reactivation" coefficient R defined as

$$\omega_s = \omega_s^o(1 - R), \tag{3}$$

where R denotes the probability that the muon — in collisions with nuclei of the traversed matter — is shaken off. R is expected to be slightly dependent on the gas density. The theoretical predictions of sticking and reactivation (at $\phi = 0.17$ where ϕ is the density normalized to liquid hydrogen density) are [2]:

$$\begin{aligned} \omega_s^o(\mathrm{th}) &= (0.92 \pm 0.01)\%, & (4) \\ R(\mathrm{th}) &= 0.29 \pm 0.03, & (5) \\ \omega_s(\mathrm{th}) &= (0.65 \pm 0.03)\%. & (6) \end{aligned}$$

The theory value (6) for final sticking ω_s is by about 50% larger than what previous experiments at LAMPF and PSI have reported from results of indirect slope measurements [2]. This discrepancy was one of the motivations to perform the present experiment which aims for the first time at a direct observation of final sticking ω_s.

The experimental setup is described in detail in refs. [3, 4]. Muons are stopped in a special ionization chamber (IC) developed in Gatchina. The IC is filled with a mixture of hydrogen isotopes at 160 bar pressure. It acts simultaneously as fusion chamber and as active detector of muons and charged fusion products. The negative charges from ionizing particles drift in a strong electric field (50 kV/cm) during 2.2 μs towards a modular anode with 19 separate readout channels. The signals are recorded by flash ADC's over a period of several muon life times (10μs). The IC operates at a condition of **large recombination** which strongly depends on the ionization density produced by the charged particle tracks. This effect is used to separate the sticking events (singly charged $\alpha\mu$) from normal fusions (doubly charged α particles) by their charge deposited on the anode. The originally produced charges are in both cases about 3.5 MeV, while after recombination they are only ~ 1.8 MeV ($\mu\alpha$) and ~ 1.2MeV (α), respectively.

The main result of the experiment performed in 1992 is displayed in fig. 1. It shows the energy spectrum of single fusion events. A pronounced $\alpha\mu$ peak, well distinguished from α and $\alpha\alpha$ events is observed. The spectrum is cleaned by the requirement of a muon-decay electron detected by a plastic counter array around the IC in a delayed time window ranging from 0.2 to 4.5 μs after the fusion event. This procedure removes muon capture events (e.g. $\mu\mathrm{N} \rightarrow 3\alpha + 2\mathrm{n} + \nu$), because there is no muon decay after capture. Such background was indeed present from muons which were transferred to N_2 impurities and from ${}^3\mathrm{He}\mu$ atoms formed after pdμ fusion.

The fit of the spectrum fig. 1 depends slightly on the assumptions about the theoretical values either of initial sticking ω_s^o or of reactivation R, since one of them had to be kept fixed. The results on direct sticking are [5]

(a) $\omega_s^o = 0.92\%$ (fixed) R free: $\omega_s(\mathrm{exp}) = (0.54 \pm 0.04\ \mathrm{stat.} \pm 0.03\ \mathrm{syst.})\%$,

(b) $R = 0.31$(fixed), ω_s^o free: $\omega_s(\mathrm{exp}) = (0.57 \pm 0.03\ \mathrm{stat.} \pm 0.03\ \mathrm{syst.})\%$.

The energy resolution during the 1992 run was so good that the visible left tail of the $\alpha\mu$ line in fig. 1 was even sensitive to muon reactivation events (stripping). The visible part of the spectrum contains those stripped $\alpha\mu$ events, that had at the moment of stripping energies $E_{\alpha\mu} \leq 2$ MeV, while those with $E_{\alpha\mu} > 2$ MeV are covered under the α peak. The fit of all events in the α-free part of the energy spectrum gives the following assignment of "visible sticking" [5]:

$$\omega_s + \delta(\omega_s^o - \omega_s) = (0.75 \pm 0.03\ \mathrm{stat.} \pm 0.03\ \mathrm{syst.})\%. \qquad \text{(exp.)}$$

This result is consistent with the theoretical prediction using the values from expr. (4) and (5):

$$\omega_s + \delta(\omega_s^o - \omega_s) = (0.78 \pm 0.03)\%. \qquad \text{(theory)}$$

Together with a value of

$$\omega_s(\mathrm{exp}) = (0.57 \pm 0.07\ \mathrm{stat.} \pm 0.02\ \mathrm{syst.})\% \qquad \text{(SMM)}$$

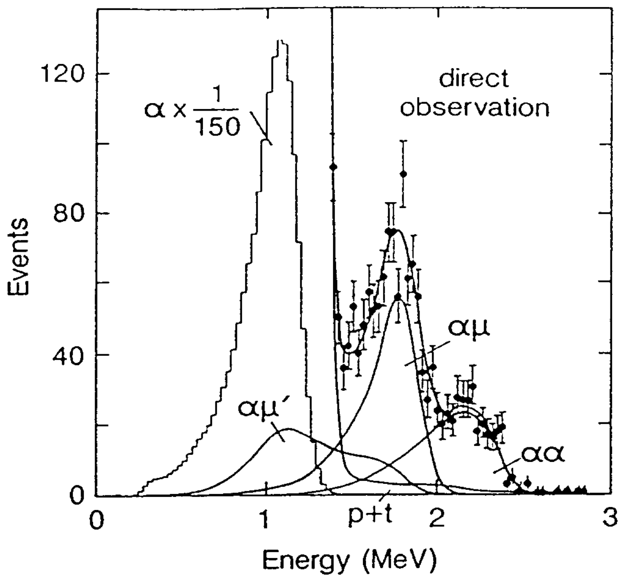

Fig. 1: Data from the 1992 PSI experiment: Direct observation of sticking showing in the upper energy region the peaks for "final" sticking ($\alpha\mu$), reactivation ($\alpha\mu'$) and pile-up ($\alpha\alpha$), see also ref. [5]. The small flat tail above the α peak is mainly background from the $dd\mu \to p + t + \mu$ fusion reaction. The curves represent the fit of M.C. generated functions to the data with $R = 0.31$.

from an evaluation of the data [6] by the "survived-muon method" (SMM) [7] the new PSI result on final sticking at density $\phi = 0.17$ (160 bar) becomes

$$\omega_s(\exp) = (0.56 \pm 0.04)\%. \tag{PSI - 1992 average}$$

This value is by about 14% or two standard deviations smaller than the theoretical prediction (eq. (6)). The discrepancy is still substantial, but smaller than what the indirect slope measurements at higher dt density ($0.97 \leq \phi \leq 1.45$) have indicated:

$$\begin{aligned} \omega_s(\exp) &= (0.48 \pm 0.02\,\text{stat.} \pm 0.04\,\text{cal.}),\% && \text{(PSI – 1987 [2])} \\ \omega_s(\exp) &= (0.43 \pm 0.05)\%. && \text{(LAMPF – 1989 [8])} \end{aligned}$$

Both of these data sets differ by more than three standard deviations from the theoretical (high density) expectation $(0.61 \pm 0.03)\%$.

In conclusion, $\alpha\mu$-sticking ω_s in d$t\mu$ fusion was for the first time directly observed. A value is now established, slightly lower than theory, limiting the possible fusion output of μCF to a value $X_c \leq 200$ per muon.

[1] C. Petitjean, Nuclear Physics **A543** (1992) 79c.
[2] C. Petitjean et al., Proc. μCF'92 (Uppsala, June 1992), to be published, see PSI PR-92-31.
[3] P. Ackerbauer et al., PSI Nuclear and Particle Physics Newsletters 1989, p. 70 and 1990, p. 50.
[4] C. Petitjean et al., Muon Cat. Fusion **5/6** (1990/91) 261; T. Case et al., ibid. p. 327, D.V. Balin et al., ibid. p. 481, K. Lou et al., ibid., p. 525.
[5] T. Case et al., Proc. *μCF'92* (Uppsala,1992), to be published.
[6] K. Lou et al., Proc. *μCF'92* (Uppsala, 1992), to be published, see PSI-PR-93-02.
[7] A.A. Vorobyov, Muon Cat. Fusion **2** (1988) 17; D.V. Balin et al., ibid. vol. **7** (1992) 1.
[8] S.E. Jones et al., Proc. *μCF'92* (Uppsala,1992), to be published.
[9] W.H. Breunlich et al., Phys. Rev. Lett. **58** (1987) 329.

2.1.16 Recoil detection at the Indiana University Cooler Ring

J. Homolka, R. Schneider, R.D. Bent [a], J. Blomgren [a], Y. Chen [a], H. Nann [a], T. Rinckel [a],
C. Sun [a], P. Heimberg [b], R.E. Segel [b], Z. Yu [b], J. Brown [c], E. Jacobsen [c], G. Hardie [d],
P. Pancella [d], K.E. Rehm [e]
[a] Indiana University Cyclotron Facility
[b] Northwestern University
[c] Princeton University
[d] Western Michigan University
[e] Argonne National Laboratory

During 1992 the setup of a recoil detection facility [1] at the Cooler ring of the Indiana university cyclotron facility (IUCF) has been completed. It was used in a beamtime in Dec. 92 and Feb. 93 to measure proton induced single pion production on carbon at 166, 200, 250 and 295 MeV incident energy. To search for double pion production also beam energies of 330 and 350 MeV were used.

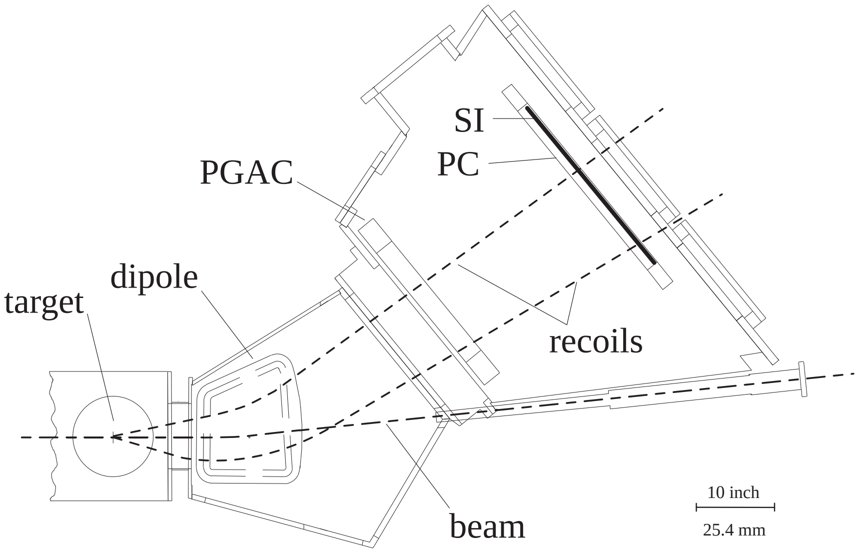

Fig. 1: Setup of the detecting system.

Figure 1 shows the detector setup. The target consists of a $5\mu g/cm^2$ carbon fiber. After a fill cycle of the ring, it is moved into the beam by a linear motor. Its speed is regulated by a feedback loop to get a constant reaction rate during 15 seconds until the beam is used up. A 6^o bending magnet, which is part of the ring, separates the low rigidity recoils from the circulating protons. To achieve a good momentum resolution, the magnet has a large field area, extending to the inner side of the Cooler ring. To accept a large vertical angular range, the dipol has a gap of 20cm. A large vacuum box, containig the detectors, is mounted at the exit port of the dipol vacuum chamber. A parallel grid avalanche counter (PGAC) measures the position in x– and y–direction. A proportional counter (PC) is located 60 cm behind the PGAC to measure dE/dx. An array of 24 large area (5x5 cm^2) silicon strip detectors inside the housing of the PC measures the position in x–direction (1mm resolution) and the residual energy E_{rest} (130 keV

FWHM resolution). For a time of flight measurement the PGAC is used as start and the silicon detector as stop detector.

The readout system for the silicon detector array was developed at the accelerator laboratory of Munich [2]. It is especially designed to achieve good timing and energy resolution for low energetic ions ($\sim$ 0.5 MeV). The ion implanted p layer of the pin diode type detector is structured with 50 strips 1mm wide and 50mm long. Each strip is connected to an amplifier followed by a discriminator. The 50 discriminator outputs belonging to one detector are connected to a resistor chain which can be read out at its two ends by charge sensing ADCs. Since only single hit events are expected on the whole silicon array, the signals are further multiplexed by switching only the chain of the responding detector to the output lines. The comparator thresholds can be as low as 500 keV deposited energy for a strip capacity of 16pF. To readout the array a total of 1200 discriminator channels are necessary. The position readout electronic and multiplexers are mounted directly behind the silicon detectors in the gas volume of the PC. The energy and timing information is generated from the signal taken form the rearside of the detector using an improved version of the preamplifier – shaper board developed by M. Ciric et al. [3]. During the two data taking runs the system operated without any problems. The nuclear charge Z of the ions is determined from dE/dx measured in the PC and the total energy given by the sum of the energy loss in the PC and the residual energy measured in the silicon detector array. Figure2 shows typical dE vs. E spectrum, which is dominated by ions with Z < 6, produced by proton induced spallation reactions in the carbon target.

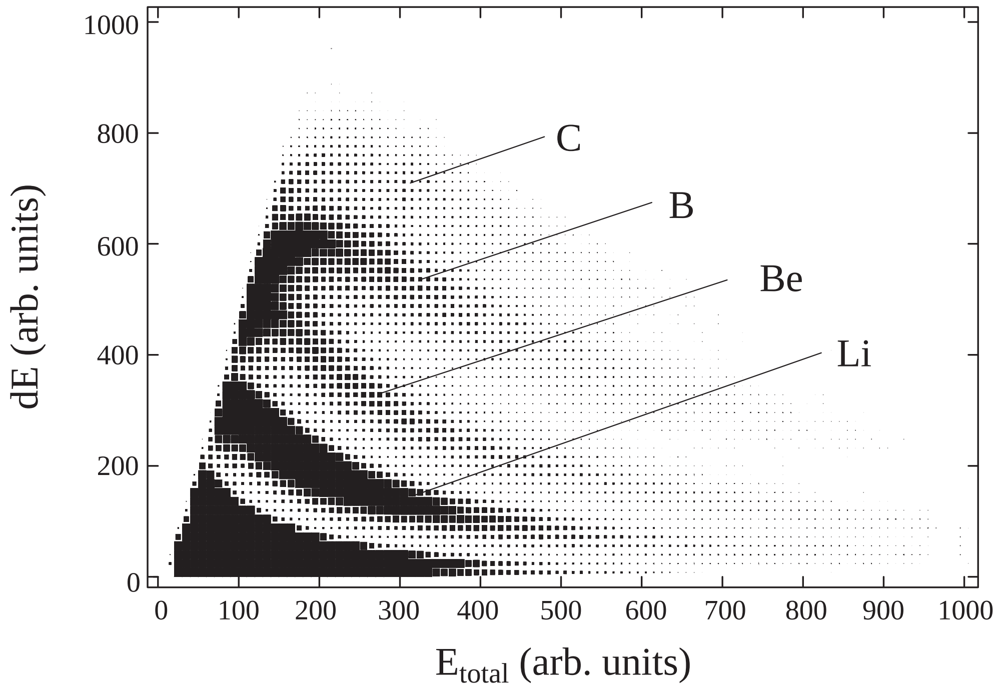

Fig. 2: Spectrum of total energy ($E = E_{rest} + dE$) vs. energy loss (dE).

To further identify the ions their mass is calculated from the total energy and the time of flight $A \sim E/v^2$. As can be seen in figure 3 for Be ions, there is only a small dependency of the calculated ion mass on the total energy, since the calibration constants are already rather accurate. The next step in analysis will be the calibration of the recoil rigidity, calculated from the position and angle information by a backtracing program.

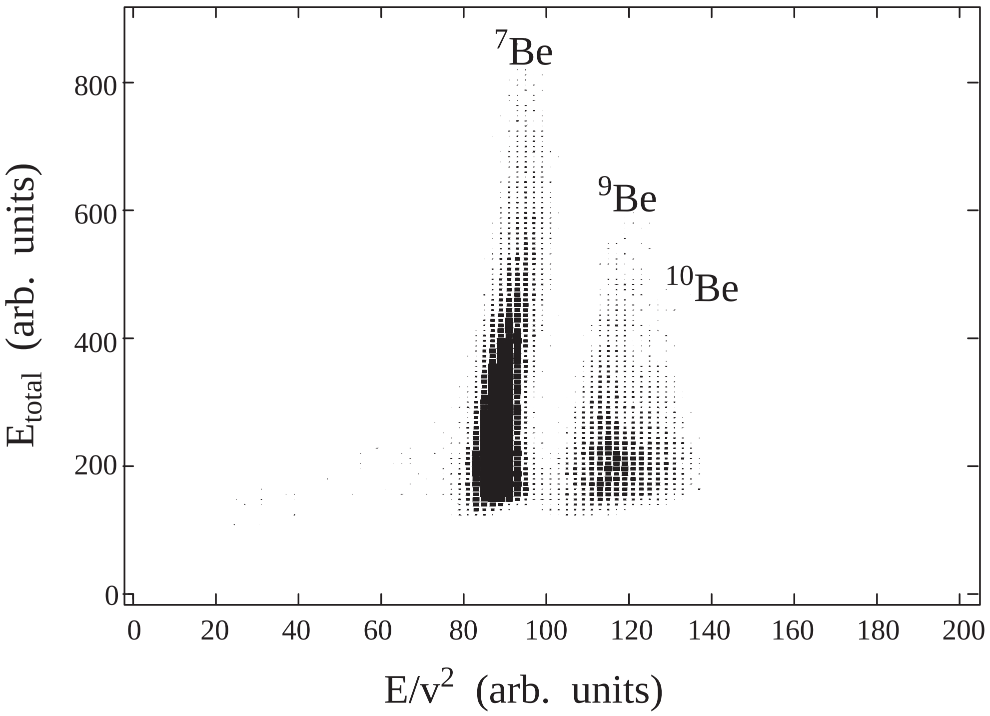

Fig. 3: Spectrum of ion mass $A \sim E/v^2$ vs. E for Be Isotopes

[1] J. Homolka et al., Jahresbericht 90, p. 210.
[2] J. Homolka, R. Schneider, A. Gillitzer, Jahresbericht 91, p. 160.
[3] M. Ciric, J. Friese, H.J. Körner, M.R. Maier, Jahresbericht 91, p. 151.

2.1.17 Signature of a neutron halo in ^{232}Th from antiproton absorption

J. Jastrzebski [a], H. Daniel, T. von Egidy, A. Grabowska [a], Y.S. Kim, W. Kurcewicz [b],
P. Lubinski [a], G. Riepe [c], W. Schmid, A. Stolarz [a], S. Wycech [d]
[a] Heavy Ion Laboratory, Warsaw University, Warsaw, Poland
[b] Institute of Experimental Physics, Warsaw University, Warsaw, Poland
[c] Forschungszentrum Jülich, D-5170 Jülich, Germany
[d] Soltan Institute for Nuclear Studies, Warsaw, Poland

During our studies of the excitation energy acquired by nuclei after the annihilation of stopped antiprotons [1] we have discovered a new method for the investigation of the neutron to proton density ratio in the nuclear periphery. This method is shortly described below.

After the annihilation of a stopped antiproton on the nuclear surface a fraction of the created particles (mainly pions) enters the nuclear volume and initiates an intranuclear cascade. Some fast nucleons are promptly emitted and the remaining part of the absorbed annihilation energy heats the nucleus so that it evaporates nucleons or heavier clusters, or fissions. As in the usual deep spallation or fission processes, heavy reaction residues are formed and can be detected using classical radiochemical methods. Two reaction residues of interest for the method proposed are the (Z_t,N_t-1) and (Z_t-1,N_t) nuclei, where Z_t and N_t are target proton and neutron numbers, respectively. It is expected that to produce these isotopes the antiproton annihilates on a neutron or proton in the far periphery of the nucleus, all produced pions miss the nucleus and the product is left with an excitation energy lower than the nucleon binding energy. The determination of the relative yields for the production of (Z_t,N_t-1) and (Z_t-1,N_t) nuclei should therefore be a sensitive method for the detection of differences between neutron and proton concentration in the nuclear stratosphere.

	Nuclei per 1000$\overline{p}$			
	Experiment		Theory, INC	
$^{231}Th(\overline{p}n)$	100 ± 27	113	19.5	33
$^{231}Ac(\overline{p}p)$	12.9 ± 1.6		13.3	
$N(\overline{p}n)/N(\overline{p}p)$	7.8 ± 2.2		1.5	

$$f(peripheral) \overset{\text{def}}{=} \frac{N(\overline{p}n)}{N(\overline{p}p)} \cdot \frac{Ima_p}{Ima_n} \cdot \frac{Z_t}{N_t} = (7.8 \pm 2.2) \cdot \frac{1}{0.63} \cdot \frac{90}{142} = 7.8 \pm 2.2$$

Table 1: Summary of the ^{232}Th evaluation

The method was first applied to the ^{232}Th target. Figs. 1 and 2 show the gamma-ray spectra in which the lines belonging to the (A_t-1) products are clearly observed. Table 1 gives the summary of the experimental results for the ^{232}Th target. A strong "neutron halo effect" is observed. The experimental data are also compared with intranuclear cascade calculations [2]. In the calculations quoted in this table the neutron halo effects were not included. New calculations [2]in which neutron halo effect was taken into account are in much better agreement with the experiment.

[1] J. Jastrzebski et al., Phys. Rev. **C47** (1993) 216
[2] Yc.S. Golubeva and A.S. Iljinov, private communication

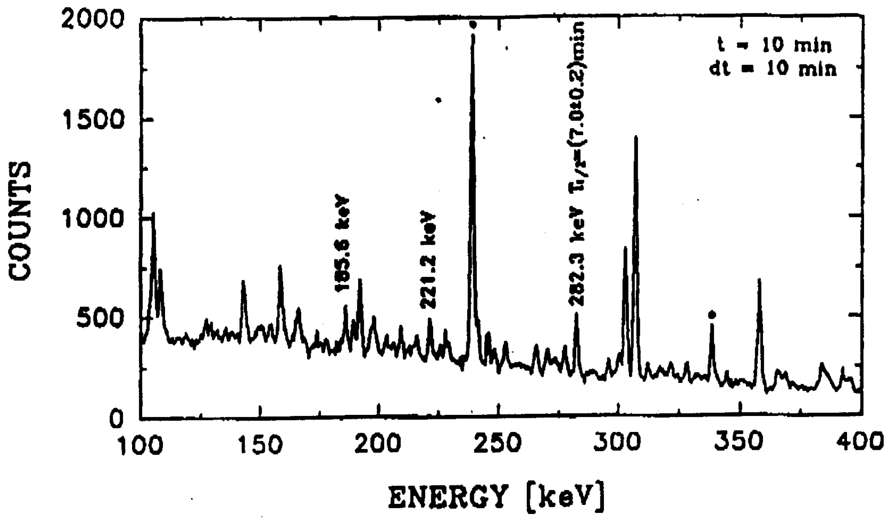

Fig. 1: The gamma ray spectrum of ^{232}Th foils irradiated by 1.3·10^{8} antiprotons and measured 10 min after the end of irradiation during 10 min with a 15 % HPGe counter. The gamma lines with indicated energies belong to the ^{231}Ac decay. Lines with asterisk are due to the natural target radioactivity. The half-life of the 282.3 keV line was determined from three consecutive spectra.

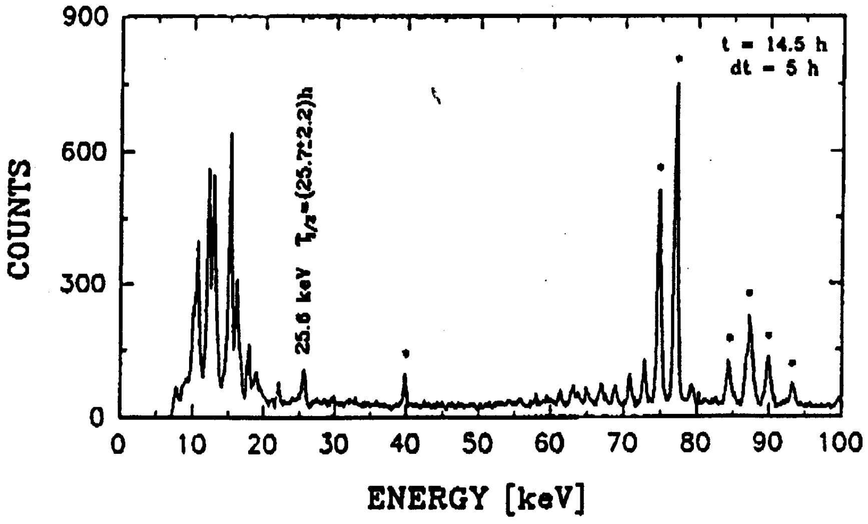

Fig. 2: The low energy gamma ray spectrum from a ^{232}Th foil measured 14.5 h after the end of irradiation during 5 h using a HPGe X-ray detector. The half-life of the 25.6 keV line, belonging to the ^{231}Th decay, was determined from three consecutive spectra. Lines with asterisk are due to the natural target radioactivity.